Distinguishing the Quasi-Decadal and Multidecadal Sea Level and Climate Variations in the Pacific: Implications for the ENSO-Like Low-Frequency Variability

Kewei Lyu

*State Key Laboratory of Marine Environmental Science, College of Ocean and Earth Sciences,
Xiamen University, Xiamen, China, and Department of Earth System Science,
University of California, Irvine, Irvine, California*

Xuebin Zhang

*Commonwealth Scientific and Industrial Research Organisation Oceans and Atmosphere,
Hobart, Tasmania, Australia*

John A. Church

Climate Change Research Centre, University of New South Wales, Sydney, New South Wales, Australia

Jianyu Hu

*State Key Laboratory of Marine Environmental Science, College of Ocean and Earth Sciences,
Xiamen University, Xiamen, China*

Jin-Yi Yu

Department of Earth System Science, University of California, Irvine, Irvine, California

(Manuscript received 3 January 2017, in final form 20 March 2017)

ABSTRACT

Low-frequency sea level variations with periods longer than interannual time scales have been receiving much attention recently, with the aim of distinguishing the anthropogenic regional sea level change signal from the natural fluctuations. Based on the available sea level products, this study finds that the dominant low-frequency sea level mode in the Pacific basin has both quasi-decadal variations and a multidecadal trend reversal in the early 1990s. The dominant sea level modes on these two time scales have different tropical structures: a west–east seesaw in the tropical Pacific on the multidecadal time scale and a dipole between the western and central tropical Pacific on the quasi-decadal time scale. These two sea level modes in the Pacific basin are closely related to the ENSO-like low-frequency climate variability on respective time scales but feature distinct surface wind forcing patterns and subbasin climate processes. The multidecadal sea level mode is associated with the Pacific decadal oscillation (PDO) and Aleutian low variations in the North Pacific and tropical Pacific sea surface temperature anomalies toward the eastern basin, while the quasi-decadal sea level mode is accompanied by tropical Pacific sea surface temperature anomalies centered in the central basin along with the North Pacific part, which resembles the North Pacific Oscillation (NPO) and its oceanic expressions [i.e., the North Pacific Gyre Oscillation (NPGO) and the Victoria mode]. The authors further conclude that the ENSO-like low-frequency variability, which has dominant influences on the Pacific sea level and climate, comprises at least two distinct modes with different spatial structures on quasi-decadal and multidecadal time scales, respectively.

Corresponding author: Kewei Lyu, lyuk1@uci.edu; Jianyu Hu, hujy@xmu.edu.cn

1. Introduction

Global mean sea level has been rising with an increasing contribution from the anthropogenic forcing (e.g., Church and White 2011; Dangendorf et al. 2015; Slangen et al. 2016). However, it is challenging to
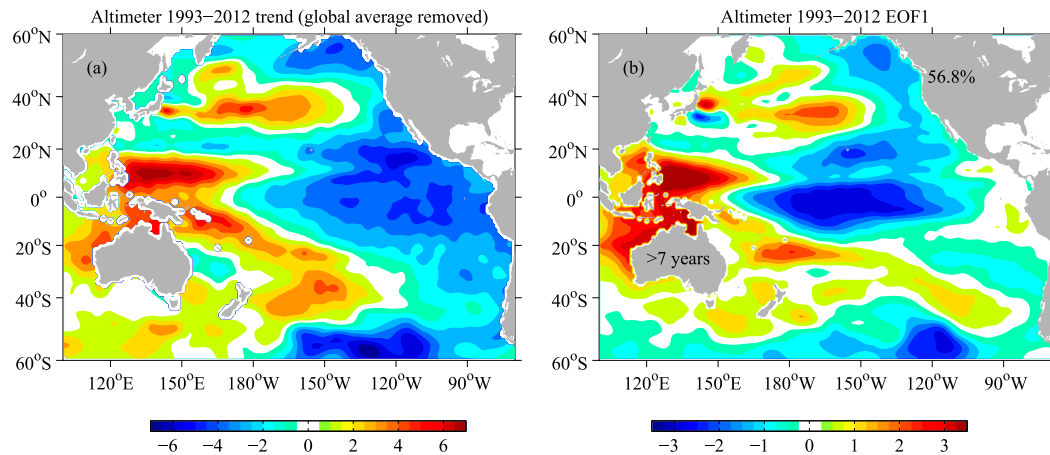
FIG. 1. (a) Altimeter-observed sea level linear trend (mm yr^{-1}) during 1993–2012 in the Pacific with the global mean (~3.2 mm yr^{-1}) removed; (b) the EOF1 pattern of low-frequency (>7 yr) sea level variations (cm) in the Pacific for the altimeter data. The percentages in (b) represent the percent of variance explained by EOF1.

identify the local or regional anthropogenic sea level change signals, which can be easily masked by the noise of natural sea level fluctuations on various temporal and spatial scales (e.g., Hu and Deser 2013; Stammer et al. 2013; Lyu et al. 2014, 2015; Carson et al. 2015). One example is the El Niño–Southern Oscillation (ENSO) variability in the tropical Pacific (TP), which induces sea level anomalies across and beyond the TP on interannual time scales (2–7 yr) (e.g., Widlansky et al. 2015).

Since the early 1990s when satellite altimeters began providing near-global sea level observations, sea level has been rising rapidly at rates up to 10 mm yr^{-1} in the western TP (around 3 times the global mean rate) but falling slightly in the eastern side of the Pacific (Fig. 1a). It has been increasingly recognized that regional sea level trend patterns calculated over such a short time period (~2 decades) are at least partly related to the low-frequency climate variability with periods longer than interannual time scales (e.g., Zhang and Church 2012; Palanisamy et al. 2015a). It remains unclear if there is any detectable anthropogenic climate change signal in the altimeter-observed sea level trend pattern (Meyssignac et al. 2012; Han et al. 2014; Hamlington et al. 2014; Palanisamy et al. 2015b; Lyu et al. 2015, 2016). Identifying the anthropogenic signal requires better understanding of the low-frequency sea level variations.

The low-frequency (usually termed "decadal" or "interdecadal"; here refers broadly to all time scales longer than interannual) climate variability in the Pacific, also known as the Pacific decadal variability (PDV; e.g., Deser et al. 2012), is characterized by the ENSO-like basin-scale patterns but with a meridionally broader tropical structure and stronger extratropical expressions than the ENSO patterns on interannual time scales (Zhang et al. 1997;

Chen and Wallace 2015). The interdecadal Pacific oscillation (IPO), originally identified as the third empirical orthogonal function (EOF) of 13.3-yr low-pass-filtered global sea surface temperature (SST) anomalies, was proposed to describe the ENSO-like interdecadal climate variability in the whole Pacific basin (Power et al. 1999; Folland et al. 1999, 2002). The IPO pattern is roughly symmetric about the equator with its North Pacific expression being similar to the Pacific decadal oscillation (PDO), defined as the first EOF (EOF1) of monthly SST anomalies in the North Pacific with time-dependent global mean removed (Mantua et al. 1997). The North Pacific Gyre Oscillation (NPGO) is another dominant climate mode in the North Pacific, derived from the second EOF of sea level anomalies in the northeastern Pacific (Di Lorenzo et al. 2008). The NPGO may also be a part of the Pacific basinwide low-frequency climate variability since the NPGO-related spatial patterns extend well beyond the northeastern Pacific (Di Lorenzo et al. 2010, 2013).

Previous studies have suggested that the low-frequency climate signals in the Pacific exist across a wide frequency range, including at least quasi-decadal (QD), bidecadal, and multidecadal (MD) time scales with periods of ~10, ~20, and 50–70 yr, respectively [see a review by Liu (2012) for details]. For example, the ENSO-like QD variations in the TP have been widely reported based on observations and coupled climate models (e.g., Brassington 1997; Knutson and Manabe 1998; Luo and Yamagata 2001; Luo et al. 2003; Lohmann and Latif 2005). In the North Pacific, the PDO and the accompanied sea level pressure (SLP) variations are dominated by bidecadal and MD signals (Minobe 1997, 1999, 2000; Zhu and Yang 2003). The MD variations manifest as the Pacific climate regime shifts about

every 20–30 yr (Deser et al. 2004), such as the well-known one around 1976/77 when the PDO switched from the negative to the positive phase. Anderson et al. (2016a) recently identified a QD spectral peak in the North Pacific from precipitation and atmospheric pressure data, probably resulting from the midlatitude ocean–atmosphere coupling (Qiu et al. 2007) or tropical Pacific forcing (Di Lorenzo et al. 2010). Observational evidence and modeling results from Tourre et al. (2001, 2005) indicated that the low-frequency SST and SLP variations in the Pacific display distinct spatial patterns on QD and bidecadal time scales, suggesting that different mechanisms could be at work.

While the studies mentioned above are usually based on atmospheric variables and SST, there are studies providing direct evidence for the low-frequency sea level variations. Chambers et al. (2012) showed that the MD (~60 yr) cycle is evident in sea level records from most tide gauges around the globe. Church et al. (2013) found an MD signal in global mean sea level in response to a range of external forcings. In addition, the sea level in the western TP has been rising rapidly over the altimeter period (Fig. 1a) but had little rising trend in the previous several decades, resulting from a combination of the long-term rising signal and an MD sea level trend reversal in the early 1990s (Merrifield et al. 2012; Qiu and Chen 2012). Feng et al. (2004, 2010, 2011) suggested that the MD sea level trend in the southeastern Indian Ocean also reversed around the same time through the oceanic connection with the western TP via the Indonesian Throughflow. In contrast, Bromirski et al. (2011) showed that the sea level off the Pacific coast of North America experienced an MD trend reversal of opposite sign (i.e., the long-term sea level rising has been slower over the recent altimeter period). Moon et al. (2013) suggested that the observed MD sea level variations in the Pacific basin can be linked to the PDO-related wind forcing.

The sea level records in the Pacific also display low-frequency signals with periods shorter than the MD time scale (e.g., QD), such as in the TP and off the western Australian coast suggested by Feng et al. (2010). In the North Pacific, Qiu (2003) found the sea level around the Kuroshio Extension displays QD variations with the dominant period of approximately 12 yr. In the South Pacific, Holbrook et al. (2011) examined the sea level and the East Australian Current along the east coast of Australia and found the ENSO- or IPO-related variations from interannual to MD time scales. Nidheesh et al. (2013) analyzed low-frequency (>7 yr) sea level variations in the tropical Indo-Pacific Ocean in an ocean general circulation model and highlighted the key role of surface wind forcing. Some studies suggested that the amplitudes of TP sea level variations over the period

band of 8–20 yr have been becoming more intense for the past 2–3 decades (Feng et al. 2010; Han et al. 2014; Moon et al. 2015).

Although the observed or modeled sea level variations in the Pacific have been linked to the major climate modes such as the ENSO, PDO, NPGO, or IPO [see a recent review by Han et al. (2017)], the basin-scale low-frequency sea level variability patterns and preferred time scales as well as the related climate processes have not been well characterized. It is also unclear if the currently available sea level products agree on the space–time features for low-frequency sea level variations in the Pacific. In this study, we aim to identify the features and mechanisms of the dominant modes of low-frequency sea level variations in the Pacific Ocean with periods longer than interannual time scales. Based on the available sea level products, we first show that the dominant low-frequency sea level mode in the Pacific basin is characterized by both QD and MD signals with different sea level anomaly patterns on these two time scales (section 3). We further discuss similarities and differences between the SST, SLP, and wind patterns associated with the QD and MD sea level modes (section 4). In section 5, we verify that the ENSO-like low-frequency variability, which has a dominant influence on the Pacific sea level, exhibits distinct spatial patterns on QD and MD time scales with different climate processes and mechanisms being involved.

2. Data and methodology

In this study, we analyzed monthly sea level data from the following four sources: the satellite altimeter observations from 1993 to 2014 produced by the CSIRO Sea Level Group (2015), the upper-ocean (0–1500 m) steric sea level over 1945–2012 calculated from the objectively analyzed temperature and salinity gridded data (FRCGC/JAMSTEC 2005; Ishii and Kimoto 2009); the European Centre for Medium-Range Weather Forecasts (ECMWF) Ocean Reanalysis System, version 4 (ORAS4; ECMWF 2012; Balmaseda et al. 2013), from 1958 to 2014; and the hindcast simulations covering the period 1950–2011 from the eddy-resolving Ocean General Circulation Model for the Earth Simulator (OFES; JAMSTEC 2015; H. Sasaki et al. 2004, 2008).

The objectively analyzed subsurface temperature and salinity data are available at 24 levels in the upper 1500 m with a horizontal resolution of 1° (Ishii and Kimoto 2009). Because of the sparseness of salinity observations over much of the historical period, there could be large uncertainties in the salinity field. However, since the sea level variations are primarily thermosteric in most regions of the Pacific (e.g., Köhl 2014;

Wu et al. 2017), the analysis of the thermosteric sea level based on temperature data alone gives very similar results (not shown).

ORAS4 is based on the Nucleus for European Modelling of the Ocean (NEMO) model and forced by the ECMWF atmospheric reanalysis products. ORAS4 uses the three-dimensional variational data assimilation (3D-Var) approach to assimilate observations from temperature and salinity profiles, satellite altimeter along-track sea level anomalies, and global mean sea level variations, SST, and sea ice. The ORAS4 product has a horizontal grid of about 1° in the extratropics and the meridional resolutions are gradually refined to ⅓° at the equator.

The OFES is based on the Modular Ocean Model, version 3 (MOM3). The model covers a near-global domain between 75°S and 75°N with a horizontal resolution of 0.1°. There are 54 vertical levels from the ocean surface to realistic bottom topography. The Boussinesq and hydrostatic approximations are adopted. After 50-yr spinup integration with climatological forcing, a hindcast integration was conducted with daily atmospheric forcing based on the National Centers for Environmental Prediction (NCEP)–National Center for Atmospheric Research (NCAR) reanalysis (NOAA/NCEP 1994; Kalnay et al. 1996).

The SST data over 1854–2014 are from the National Oceanic and Atmospheric Administration (NOAA) Extended Reconstructed SST (ERSST; Smith et al. 2008; NOAA/NCEI 2015) dataset. The atmospheric data analyzed in this study are from the NCEP–NCAR reanalysis from 1948 to 2015, the Japanese 55-year Reanalysis (JRA-55; JMA 2013; Kobayashi et al. 2015) from 1958 to 2013, and the NOAA Cooperative Institute for Research in Environmental Sciences (CIRES) Twentieth Century Reanalysis (20CR; Compo et al. 2011, 2015) available from 1851 to 2014.

At each grid point, monthly anomalies were first derived by removing the monthly climatology. Our results are insensitive to different choices of base period that used to define the climatology. Then the data were linearly detrended at each grid point. The time-dependent global mean sea level time series was also subtracted from the sea level field since this study focuses on the regional deviations. A 7-yr Lanczos low-pass filter (Duchon 1979) was used to derive the low-frequency signals. Similar cutoff periods (6–8 yr) were usually used to remove interannual signals (Zhang et al. 1997; Deser et al. 2012; Zhang and Church 2012; Nidheesh et al. 2013; Han et al. 2014; Sullivan et al. 2016). The Lanczos filtering works well to suppress the Gibbs oscillation and has a relatively sharp cutoff in its response function (not shown). We have removed the last two years of the filtered data to reduce the end point effect.

The dominant modes of sea level variations in the Pacific were identified using the EOF method. We also applied the singular value decomposition (SVD) analysis to the cross-covariance matrix of two data fields (e.g., sea level and SST) with the aim to find the leading modes of their covariability. All spatial fields of the data have been weighted with the square root of the cosine of latitude before the EOF or SVD analysis (Wallace et al. 1992). We normalized the derived EOF principal component (PC) or SVD time series to unit variance and then multiplied the spatial field by the corresponding standard deviation value. This procedure makes the EOF or SVD spatial patterns to have same unit as the original data and thus show the real amplitude represented by the EOF or SVD modes.

3. The dominant modes of low-frequency sea level variations in the Pacific

a. Low-frequency sea level EOF1 over altimetry and longer periods

The EOF analysis was first applied to the 7-yr low-pass-filtered sea level anomalies in the Pacific basin (60°S–60°N, 100°E–70°W, including part of the southeastern Indian Ocean). Note that the data have been linearly detrended over the respective analysis period before the EOF analysis. The altimeter EOF1 has a similar large-scale pattern (Fig. 1b) to the altimeter-observed trend pattern (Fig. 1a) with the spatial correlation of 0.69 over the Pacific basin, indicating the potential connection between the altimeter-observed regional sea level trend and the dominant mode of low-frequency sea level variations in the Pacific. The higher-than-normal sea level or positive trends are in the western TP, the southeastern Indian Ocean, and most of the midlatitudes, while the lower-than-normal sea level or negative trends are in the central–eastern TP, high latitudes of the South Pacific (south of 50°S), and off the Pacific coast of the Americas (Fig. 1). Despite similar large-scale distributions, one major difference between the altimeter trend pattern and low-frequency EOF1 pattern lies in the TP, where the negative sea level anomalies or trends cover the central–eastern TP for the trend pattern (Fig. 1a) but are mainly confined in the central TP (roughly between 160°E and 100°W) for the low-frequency EOF1 pattern (Fig. 1b). We also analyzed the OFES, ORAS4, and steric sea level data after 1993 and found that their EOF1 patterns over the altimeter period show a negative sea level anomaly center in the central TP (Figs. 2a–c) similar to the altimeter EOF1 pattern (Fig. 1b), with the spatial correlations in the TP (between 20°S and 20°N) of 0.79, 0.99, and 0.94, respectively.
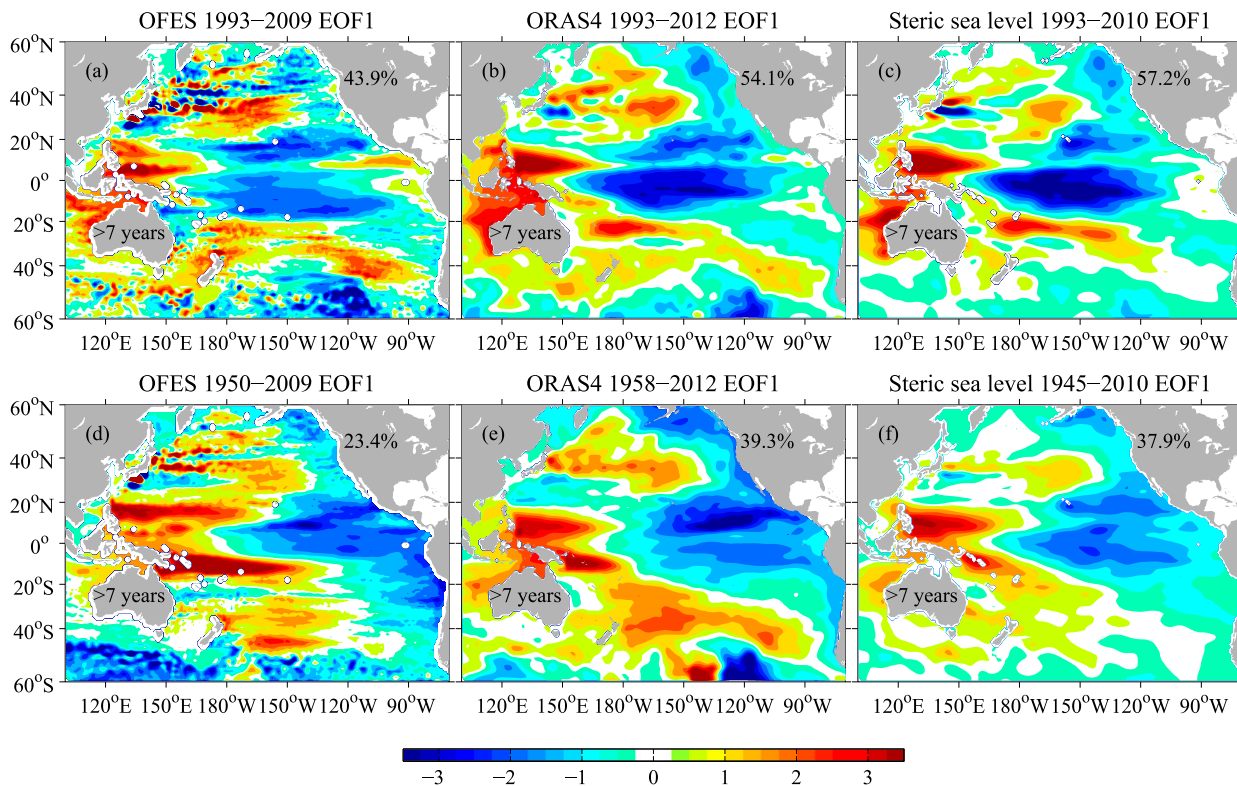
FIG. 2. The EOF1 patterns of low-frequency (>7 yr) sea level variations (cm) in the Pacific from the (a),(d) OFES, (b),(e) ORAS4, and (c),(f) steric sea level based on (top) data after 1993 and (bottom) data over the full available period. The percentages in each panel represent the percent of variance explained by EOF1.

Although the low-frequency EOF1 patterns over the altimeter period show consistent features in different sea level products (Figs. 1b and 2a–c), the altimeter period of about two decades may not be long enough for identifying the low-frequency variability pattern, as pointed out by Zhang and Church (2012). Frankcombe et al. (2015) suggested at least 50 yr of data are required to obtain a robust pattern for low-frequency sea level variations. When the EOF analysis was performed with the OFES, ORAS4, and steric sea level datasets over their full periods (~60 yr), the low-frequency EOF1 patterns show that the negative sea level anomalies in the TP are displaced eastward (Figs. 2d–f), similar to the altimeter trend patterns (Fig. 1a) with the spatial correlations in the TP of 0.77, 0.94, and 0.94, respectively. Note that the analysis periods for the OFES, ORAS4, and steric sea level are slightly different (Fig. 2), depending on data availability. Conducting EOF analysis over an overlapping period (e.g., 1993–2009 or 1960–2009) shows very similar results.

The low-frequency EOF1 based on the relatively longer data (Figs. 2d–f) seems to be more reliable to represent the dominant mode of low-frequency sea level variations in the Pacific. However, it is still

unclear what processes determine the different patterns for the dominant low-frequency sea level mode derived over different data lengths (Figs. 2a–c vs Figs. 2d–f). Given that the satellite altimeter is the only source of direct sea level measurements with continuous quasi-global coverage, it is also of great importance to understand and reconcile the inconsistencies between results from the altimeter (Fig. 1b) and other sea level products (Figs. 2d–f).

The EOF results should be examined using both spatial and temporal information. The low-frequency EOF1 PC (PC1) time series based on sea level data after 1993 exhibit nearly two complete cycles from 1993 to the 2010s (see black line in Fig. 3a for the altimeter PC1), indicating a possible QD period of approximately 10 yr (Fig. 4a). The correlations between PC1 time series from altimeter and other datasets (not shown) are larger than 0.97 over 1993–2011. Clearly, the data over around two decades (e.g., the altimeter sea level data since 1993) cannot resolve climate variations with periods longer than two decades. The PC1 time series over the full period (~60 yr) of longer sea level datasets exhibit similar QD variations and also a declining trend prior to the early 1990s and a rising trend afterward (Fig. 3a).
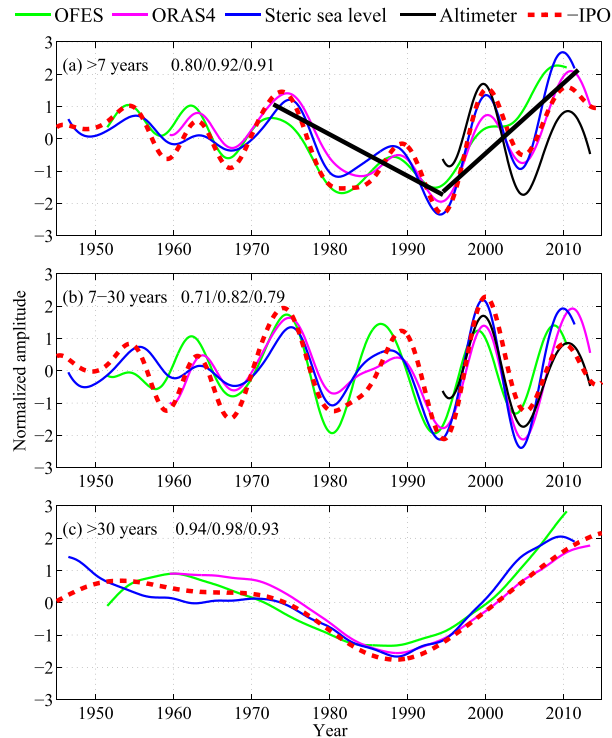
FIG. 3. The EOF1 time series of sea level variations in the Pacific on time scales (a) >7, (b) between 7 and 30, and (c) >30 yr from the altimeter (black), OFES (green), ORAS4 (magenta), and steric sea level (blue). The reversed IPO index time series on corresponding time scales are also shown (red dashed lines). The numbers at the top left in each panel indicate the correlations between the reversed IPO index and the EOF1 time series on corresponding time scales for OFES, ORAS4, and steric sea level. The thick black lines in (a) roughly mark the trend reversal before and after the early 1990s.

These temporal features are reflected in the spectrum analysis, which shows a significant peak on the QD time scale between 10 and 14 yr and also enhanced variance on the MD time scale with periods longer than approximately 20 yr (see black lines in Figs. 4b–d). Therefore, the EOF1 of 7-yr low-pass-filtered sea level in the Pacific over the short altimeter period captures only the dominant mode of the QD signal (Figs. 1b and 2a–c). But over the full period of the longer sea level products, a mixed mode with contributions from both QD and MD signals is present (Figs. 2d–f). This raises an interesting question: Can these longer sea level products achieve better agreement with the altimeter data when the MD signal is removed?

b. Separating QD and MD sea level signals

To isolate the QD signal from the MD and interannual signals, we applied the EOF analysis to the 7–30-yr bandpass-filtered sea level data from the OFES, ORAS4, and steric sea level. Using different cutoff periods (e.g., 7–20 or 10–20 yr) yields similar results (not shown). The PC1 time series display mainly QD variations (Fig. 3b), indicated by a prominent single peak between 10 and 14 yr in the corresponding power spectra (see red lines in Figs. 4b–d). These QD PC1 time series (Fig. 3b) are highly correlated with the low-frequency PC1 time series (Fig. 3a) on time scales of 7–30 yr, with the correlations being 0.82, 0.92, and 0.95 for OFES, ORAS4, and steric sea level, respectively. In this case, the EOF1 (7–30 yr) patterns show a negative sea level anomaly center in the central basin of the TP (Figs. 5a–c) similar to the low-frequency (>7 yr) EOF1 patterns derived over the short altimeter period (Fig. 1b), with high spatial correlations in the TP (between 20°S and 20°N) of 0.83, 0.93, and 0.91 for OFES, ORAS4, and steric sea level, respectively. Therefore, the dominant patterns for QD sea level variations in the Pacific basin are consistent among the various sea level products analyzed in this study, despite having different time lengths (Figs. 1b and 5a–c). The QD sea level variability patterns identified here share very similar features with the QD (~12 yr) variance distributions for the upper-ocean heat content, which also have the maximum values in the western and central TP (Hasegawa and Hanawa 2003).

This basin-scale QD sea level mode could significantly influence the sea level trend patterns calculated over a short time period. For example, based on satellite altimeter observations, Lee and McPhaden (2008) showed that the sign of sea level trends over 1993–2000 and 2000–06 almost reversed in much of the Pacific region. The timing of this trend reversal coincides with the QD PC1, which also has opposite sign of trends over short periods before and after 2000 (Fig. 3b). The sea level trend patterns over these two periods closely resemble (or mirror) the EOF1 patterns of QD sea level variations in the Pacific, including the center of action in the central TP (Figs. 1b, 2a–c, and 5a–c), as also noted by Han et al. (2014). Recently Hamlington et al. (2016) reported a shift in Pacific sea level in the past several years with sea level rising (falling) in the eastern (western) Pacific, which is consistent with a decline in the altimeter QD PC1 since around 2010 (see the black line in Fig. 3b). However, attributing such a shift at the end of a time series to the QD or MD climate signal is highly uncertain.

We performed the EOF analysis with the 30-yr low-pass-filtered sea level data to check if the sea level datasets agree on the MD signal. The 20-yr low-pass-filtered data provide very similar results (not shown). The MD EOF1 patterns (Figs. 5d–f) have some similarities in large-scale distributions to the QD EOF1 patterns (Figs. 5a–c; e.g., positive anomalies in the western TP and the midlatitudes and negative anomalies in the eastern Pacific). However, compared with the QD EOF1 patterns (Figs. 5a–c), the
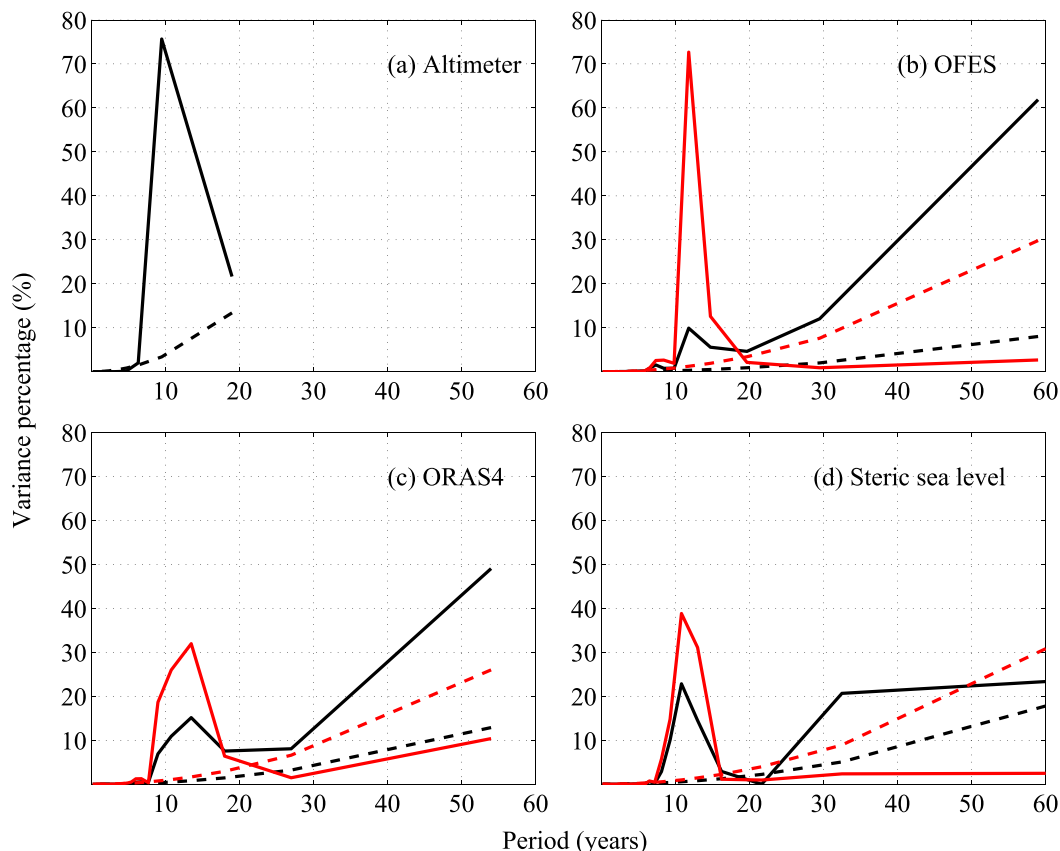
FIG. 4. Power spectra of the EOF1 time series of sea level variations in the Pacific on time scales >7 yr (black) and between 7 and 30 yr (red) for the (a) altimeter, (b) OFES, (c) ORAS4, and (d) steric sea level. The y axis is plotted as the percent of variance explained by the signal at a particular period. Dashed lines represent the 95% significance level.

MD EOF1 patterns (Figs. 5d–f) do not have a sea level anomaly center in the central TP but feature an east–west sea level seesaw structure in the TP as in the altimeter trend pattern (Fig. 1a). The MD PC1 time series for OFES, ORAS4, and steric sea level all show a declining trend prior to the late 1980s, followed by a full rebound afterward (Fig. 3c). The MD PC1 time series (Fig. 3c) closely resemble the MD component of the low-frequency PC1 time series (Fig. 3a) with the correlations being larger than 0.92. Note that the effective degrees of freedom could be largely reduced after a 30-yr filter, and thus the calculated high correlation numbers based on the filtered data should be interpreted with caution. We also noticed that although the pure MD signal has the turning point around the late 1980s (Fig. 3c), the superposition of QD cycle with a positive peak in the late 1980s and a negative peak in the early 1990s (Fig. 3b) makes the MD trend reversal appear to be in the early 1990s based on the raw or 7-yr low-pass-filtered data (Fig. 3a). Since the altimeter data from 1993 only covered the latter upswing period of the MD cycle (Fig. 3c), the altimeter-observed sea level

trends (Fig. 1a) should be viewed as a combination of both the long-term sea level change signal and the upward or downward phase of MD sea level variations (e.g., Zhang and Church 2012).

Recently there has been significant effort to detect the anthropogenic sea level change signal in the altimeter observations by removing the natural sea level variations, especially the rapid sea level rise in the western TP in the past two decades (e.g., Hamlington et al. 2014). The detection results from such an attempt should be viewed with caution because the currently available sea level products may not be good enough in quality or long enough in time length to quantify the regional MD sea level signal, although the identified MD large-scale patterns (Figs. 5d–f) and their temporal evolutions (Fig. 3c) are fairly consistent among the sea level datasets analyzed in this study. First, the sea level data barely cover only one MD cycle (Fig. 3c); thus the MD EOF1 patterns (Figs. 5d–f) represent only the leading mode of MD sea level variations in the Pacific since about 1950, which is not necessarily the typical MD sea level variability
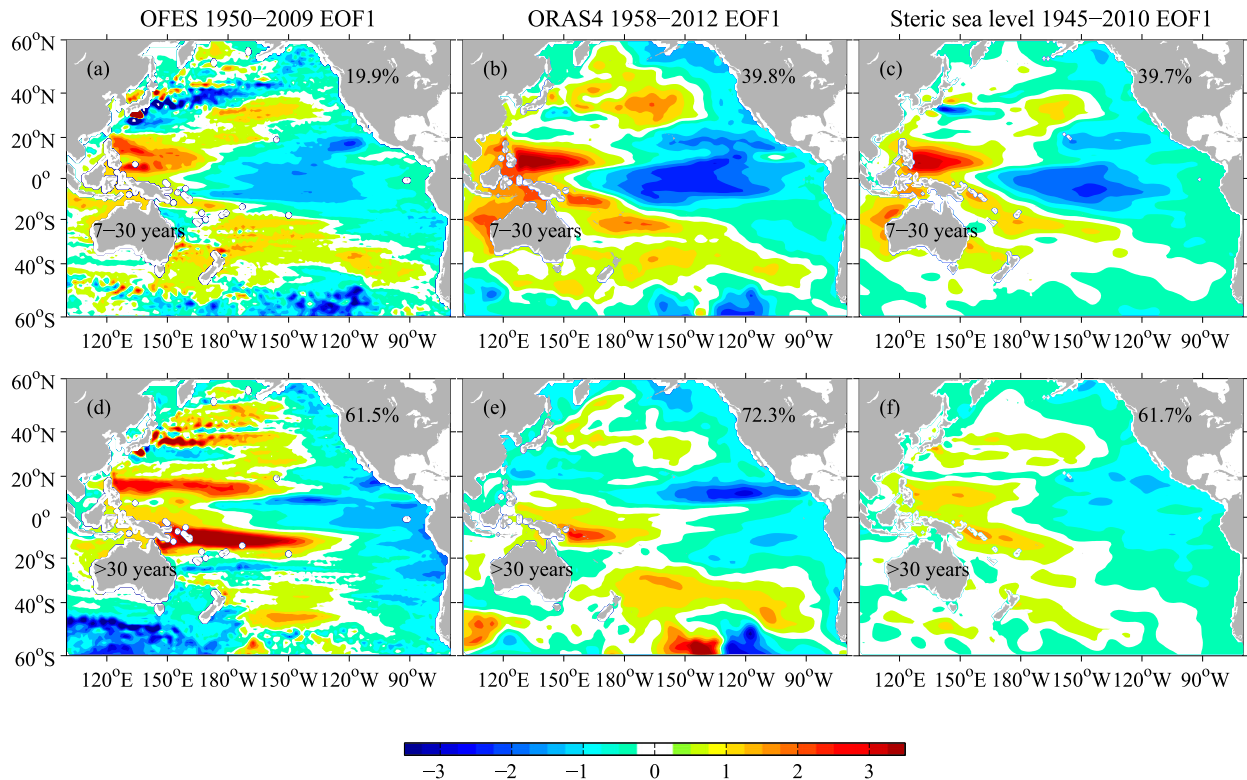
FIG. 5. The EOF1 patterns of sea level variations (cm) in the Pacific on time scales (a)–(c) between 7 and 30 yr, and (d)–(f) >30 yr from the (left) OFES, (center) ORAS4, and (right) steric sea level. The percentage in each panel represents the percent of variance explained by the EOF1.

pattern. Second, despite the large-scale consistency, the MD EOF1 patterns show large uncertainties in detail between the different sea level products. For example, the MD EOF1 patterns show local maxima of positive sea level anomalies in the northwestern TP that are located at ~15°, ~3°, and ~10°N for OFES, ORAS4, and the steric sea level, respectively (Figs. 5d–f). The magnitude of these maximum anomalies for OFES is almost twice as large as that for steric sea level and 3 times that for ORAS4. Feng et al. (2011) pointed out that the trend magnitudes of the equatorial Pacific wind before and after the early 1990s, which act as the primary forcing for the MD sea level trend reversal in the TP, also differ among available wind products. These factors cast doubt on our ability to determine the robust MD sea level variability pattern in the Pacific and thus to precisely quantify the anthropogenic regional sea level change signal from altimeter observations.

4. Atmospheric forcing patterns and origins for QD and MD sea level modes

In the previous section, we identified two distinct modes of sea level variations in the Pacific basin on QD and MD

time scales, respectively. These two sea level modes exhibit similar basin-scale patterns but also detailed differences, especially in the TP (Fig. 5). Which climate modes can these two sea level modes be linked to? Are their similarities and differences physically meaningful and also reflected in other climate fields? Can the differences in QD and MD sea level patterns be explained by the surface wind forcing differences, and which climate processes lead to distinct wind forcing patterns on these two time scales? To address these issues, we applied the SVD analysis to the cross-covariance matrix of sea level and each of the other variables (SST, SLP, sea surface wind, and wind stress curl). The SVD analyses were conducted with two different combinations of datasets: the OFES and NCEP–NCAR and the steric sea level and JRA-55. The SVD analysis based on the OFES and NCEP–NCAR aims to identify statistical connections between these two physically consistent datasets since the OFES was forced based on the NCEP–NCAR atmospheric forcing. In addition, analyzing the steric sea level and JRA-55 further verifies if these connections could also be found from the other two independent datasets.

We found that the sea level patterns from the first SVD mode (SVD1) are always very similar to those
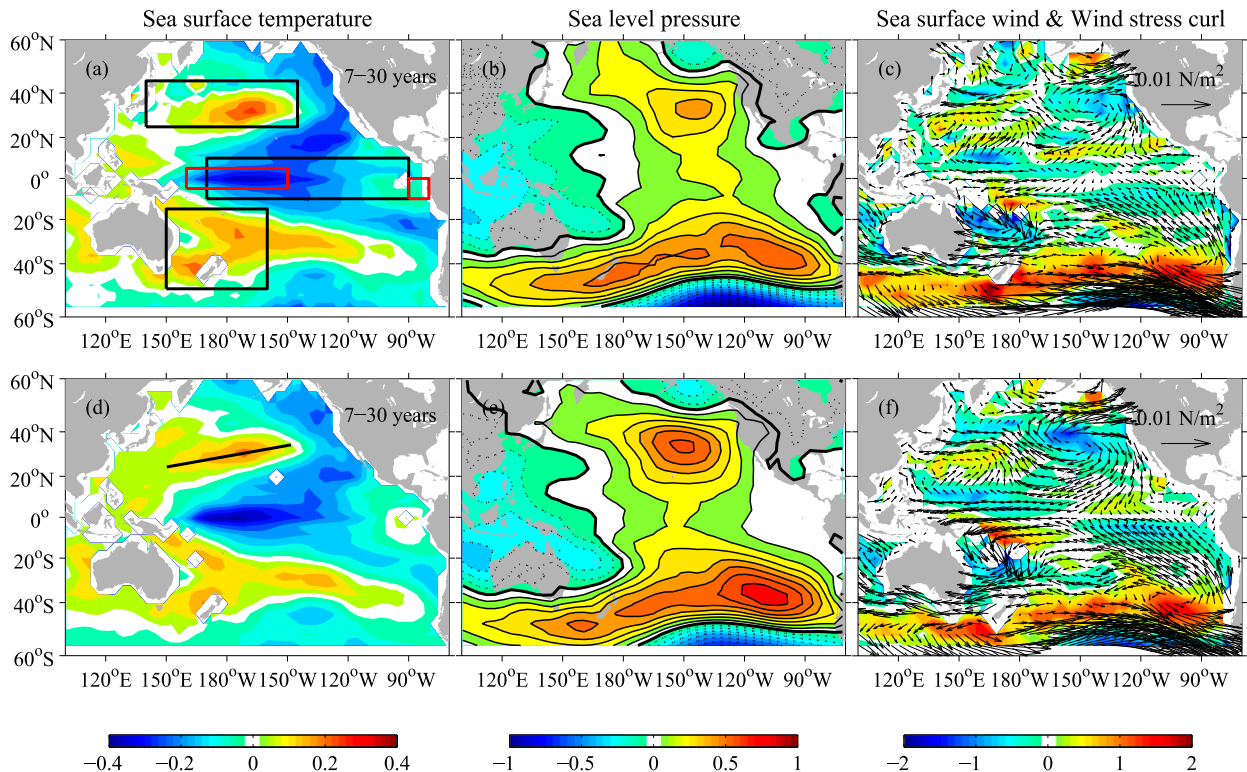
FIG. 6. The (a),(d) SST (°C), (b),(e) SLP (hPa), and (c),(f) sea surface wind stress (N m^{-2}; vectors) and wind stress curl (10^{-8} N m^{-3}; color shading) patterns corresponding to the Pacific QD sea level mode as shown in Figs. 5a–c, derived from the SVD1 of 7–30-yr bandpass-filtered sea level and each of the other variables based on (top) OFES and NCEP–NCAR data and (bottom) steric sea level and JRA-55 data. The three regions used to define the IPO index (Henley et al. 2015) are shown with black boxes in (a). The red boxes in (a) indicate the Niño-4 and Niño-1+2 regions. The black line in (d) marks the orientation of SST anomalies in the central–western North Pacific.

from the EOF1 based on sea level data only (Fig. 5) with the pattern correlations being larger than 0.90. The associated SVD1 and EOF1 time series follow each other with temporal correlations being larger than 0.90 (0.99) on time scales between 7 and 30 yr (>30 yr). Therefore, the SVD1 captures not only the dominant mode of sea level variations in the Pacific as the sea level EOF1 (Fig. 5) but also the corresponding patterns of other climate variables, including SST, SLP, sea surface wind, and wind stress curl (e.g., Fig. 6).

a. Patterns and climate processes associated with the QD sea level mode

The SVD analysis of the 7–30-yr bandpass-filtered data was used to identify the climate patterns associated with the QD sea level mode (Figs. 5a–c). The SVD1 patterns based on the pair of OFES and NCEP–NCAR or the pair of steric sea level and JRA-55 are very close to each other (Figs. 6a–c vs Figs. 6d–f) with the pattern correlations being 0.94, 0.93, and 0.82 for SST, SLP, and wind stress curl, respectively. The QD SST pattern resembles the ENSO-like low-frequency variability pattern in the Pacific (Zhang et al. 1997; Chen and Wallace 2015),

characterized by SST anomalies of one sign in the TP flanked by anomalies of opposite sign to the north and south in midlatitudes (Figs. 6a,d). Recently, Henley et al. (2015) proposed a new IPO index to describe the ENSO-like variability in the Pacific, calculated as SST differences between the average in the TP and the average in the extratropical northwest and southwest Pacific (see black boxes in Fig. 6a for the three regions). Here the unfiltered IPO index (available online at http://www.esrl. noaa.gov/psd/data/timeseries/IPOTPI/) is used to represent the ENSO-like variability in the Pacific ranging from interannual to MD time scales. The power spectrum of the unfiltered IPO index exhibits substantial power on interannual time scales, a prominent QD peak at a period of approximately 12 yr, and also enhanced power at lower frequencies (Fig. 7a). The QD spectral peak would become statistically significant when the 7-yr low-pass-filtered IPO index is used to calculate the power spectrum (not shown). Another ENSO-like variability index used by Chen and Wallace (2015), defined as the PC1 of unfiltered global or Pacific SST anomalies with time-dependent global mean removed, also has a 12-yr period component. Han et al. (2014)
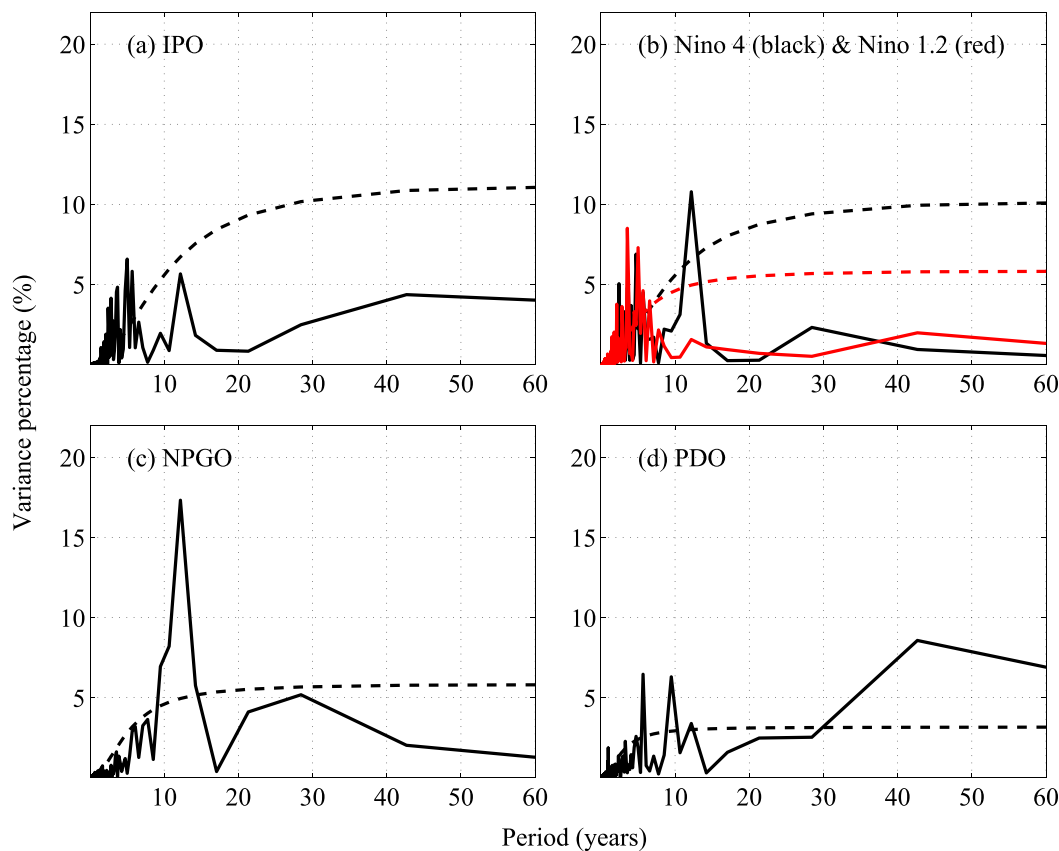
FIG. 7. Power spectra of the (a) IPO, (b) Niño-4 and Niño-1+2 SST, (c) NPGO, and (d) PDO indices since 1950. The *y* axis is plotted as the percent of variance explained by the signal at a particular period. Dashed lines represent the 95% significance level.

also showed that there is a significant QD spectral peak with periods between 10 and 15 yr for the PC1 of 8-yr low-pass-filtered SST anomalies in the Pacific. The QD SVD1 SST time series based on OFES data closely follows the 7–30-yr bandpass-filtered IPO index with a high correlation of −0.96. The sea level PC1 time series based on different sea level datasets are also related to the IPO index over the period band of 7–30 yr (Fig. 3b). These relationships suggest that the basin-scale QD sea level mode in the Pacific (Figs. 5a–c) can be linked to the ENSO-like low-frequency variability, which has a clear QD component.

One outstanding feature from the QD SST patterns (Figs. 6a,d) is that the tropical SST anomalies are located toward the central TP basin with the center in the Niño-4 region (5°N–5°S, 160°E–150°W), while the SST anomalies in the far-eastern TP are of much smaller magnitude (e.g., the Niño-1+2 region at 0°–10°S, 90°–80°W; see red boxes in Fig. 6a for these two Niño regions). The spectral analyses indicate that the QD spectral peak of approximately 12 yr is significant for Niño-4 region SST but is absent for Niño-1+2 region

SST (Fig. 7b). The QD SVD1 SST time series based on OFES data is highly anticorrelated with the 7–30-yr bandpass-filtered Niño-4 SST index (−0.87). Such connection is consistent with Behera and Yamagata (2010), who showed the TP sea level low-frequency evolutions over the altimeter period followed the low-frequency component of the El Niño Modoki index (Ashok et al. 2007). As pointed out by Weng et al. (2007), the El Niño Modoki index is also dominated by low-frequency signals on the QD time scale, similar to the Niño 4 SST index (Fig. 7b) and other indices for the ENSO events peaked in the central TP (Sullivan et al. 2016). Therefore, the QD sea level variations in the TP (Figs. 5a–c) are closely related to the central TP SST QD variations (Figs. 6a,d).

Corresponding to the positive phase of the QD sea level mode with anomalously high sea level in the western TP and low sea level in the central TP (Figs. 5a–c), the SLP patterns exhibit negative SLP anomalies over the western TP and the high latitudes and positive SLP anomalies over the central TP and the midlatitudes (Figs. 6b,e). Over the North Pacific, a region of high

pressure anomaly between 20° and 50°N and another low pressure anomaly region north of 50°N establish a north–south SLP dipole structure that resembles the North Pacific Oscillation (NPO; Rogers 1981), defined as the second EOF of SLP anomalies over the North Pacific. Note that the NPO-like SLP dipole structure on the QD time scale is less symmetric than that on interannual time scales, with the southern anomaly center of the dipole being much stronger than the northern counterpart (Figs. 6b,e). This asymmetry is consistent with the previous findings by Di Lorenzo et al. (2010) and Furtado et al. (2012) that the SLP variations over the southern pole of the NPO-like SLP dipole have greater power on the QD time scale.

The NPO-like atmospheric forcing has been linked to the NPGO (Di Lorenzo et al. 2008) and also the second EOF of SST anomalies in the North Pacific [i.e., the Victoria mode defined by Bond et al. (2003)]. The Victoria mode–like SST features can be seen in the QD SST patterns, with the southwest–northeast-oriented (marked by the black line in Fig. 6d) SST anomalies in the western–central North Pacific being surrounded by anomalies of opposite sign (Figs. 6a,d). As the oceanic expression of the NPO, the NPGO (the index is available online at http://www.o3d.org/npgo/npgo.php) shows a remarkable spectral peak at approximately 12 yr (Fig. 7c), indicating that the QD variability is a fundamental feature for the NPGO. Compared with the NPGO, the SST Victoria mode has greater interannual signals but lacks a particular QD spectral peak (Ding et al. 2015), suggesting that the SST and sea level variations could be governed by different physical processes and thus are not completely consistent with each other. In contrast, the PDO index (available online at http://research.jisao.washington.edu/pdo/PDO.latest) exhibits enhanced variance mainly on the MD time scale (Fig. 7d). The NPGO-like sea level patterns can be seen in the northeastern Pacific part of the QD sea level patterns, with positive sea level anomalies in the central North Pacific and negative sea level anomalies in the Gulf of Alaska (Figs. 5a–c), indicating the intensification of both the subtropical gyre and the Alaskan Gyre (Di Lorenzo et al. 2008). The NPGO-related SST and SLP patterns identified by Di Lorenzo et al. (2010, 2013) are also very similar to those associated with the Pacific basin QD sea level mode (Fig. 6). Therefore, the NPGO, a local sea level EOF mode in the northeastern Pacific (Di Lorenzo et al. 2008), could be viewed as the North Pacific component of the basin-scale QD sea level mode in the Pacific Ocean. It needs to be pointed out that part of the NPGO signal may arise from the northeastern Pacific internal processes that are independent from those outside the northeastern Pacific, which may not be captured by the basin-scale mode derived within the whole Pacific domain.

Several studies have suggested the surface wind forcing to be the primary driver for the regional sea level variations and changes in the Pacific (e.g., Lee and McPhaden 2008; McGregor et al. 2012; Qiu and Chen 2012; Zhang et al. 2012, 2014; Moon et al. 2013; Nidheesh et al. 2013; Palanisamy et al. 2015a). In the equatorial Pacific, the QD sea level mode is accompanied by the easterly wind anomalies to the west of 150°W and westerly wind anomalies to the east (Figs. 6c,f), consistent with the negative sea level anomaly center in the central TP (Figs. 5a–c). The easterly wind anomalies also lead to higher-than-normal sea level in the western TP through the pileup of water there. These wind anomalies are in accordance with the anomalous SLP zonal gradient in the TP, built up by one high SLP anomaly center over the central TP and the other low SLP anomaly center over the western TP (Figs. 6b,e). The two off-equator centers of positive sea level anomalies in the western TP (Figs. 5a–c) can be explained by the negative (positive) wind stress curl anomalies at around 10°N (10°S) (Figs. 6c,f) through the westward propagation of baroclinic Rossby waves (e.g., Capotondi and Alexander 2001; Capotondi et al. 2003). Along the west coast of Australia, the positive sea level anomalies are due to the oceanic connections with the western TP rather than local winds, with the local negative wind stress curl anomalies and the northward alongshore wind anomalies tending to induce negative sea level anomalies. In the northeastern Pacific, the NPGO-like sea level pattern corresponds to the NPO-like wind forcing, which induces positive wind stress curl anomalies over the Gulf of Alaska and negative wind stress curl anomalies to the south. In the South Pacific, several studies have suggested that the baroclinic ocean Rossby waves generated by wind stress curl anomalies are the primary mechanism in shaping the pattern of sea level anomalies on low-frequency time scales (Qiu and Chen 2006; Y. Sasaki et al. 2008; Holbrook et al. 2011). Besides the large-scale wind-driven dynamics, the ocean internal variability (e.g., dynamical instabilities and eddies) could also contribute to the low-frequency sea level variations, especially in the mid-to-high latitudes (Li and Han 2015; Qiu et al. 2015; Sérazin et al. 2016).

b. Patterns and climate processes associated with the MD sea level mode

The SST, SLP, sea surface wind, and wind stress curl patterns associated with the MD sea level mode (Figs. 5d–f) were derived from the SVD1 of 30-yr low-pass-filtered data (Fig. 8). The MD SST patterns (Figs. 8a,d) have similar ENSO-like low-frequency SST
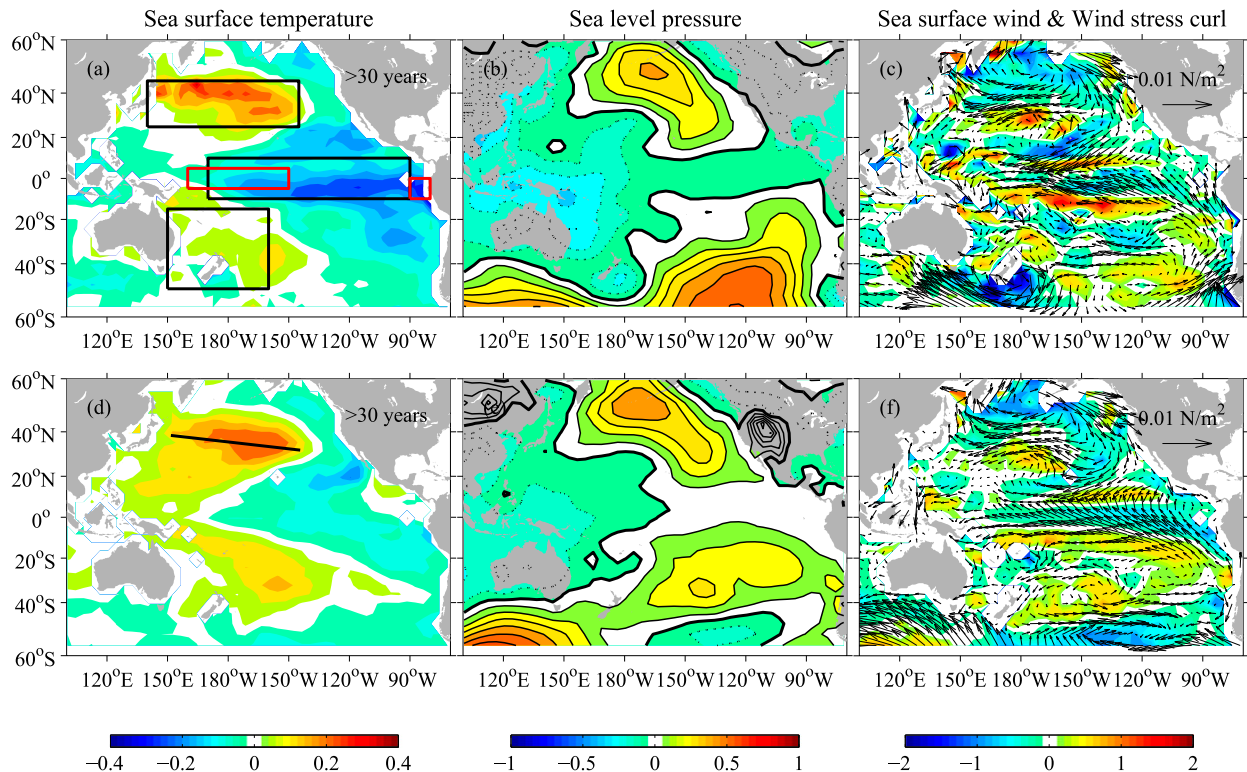
FIG. 8. As in Fig. 6, but for patterns corresponding to the Pacific MD sea level mode as shown in Figs. 5d–f, derived from the SVD1 of 30-yr low-pass-filtered sea level and each of the other variables.

patterns in the Pacific to the QD SST patterns (Figs. 6a,d), but there are also some differences, notably in the TP where the SST anomalies cover the central–eastern TP on the MD time scale but are centered in the central TP on the QD time scale. The differences in the North Pacific are subtle but significant: on the MD time scale, the SST anomalies in the western–central North Pacific are more zonally oriented (marked by the black line in Fig. 8d), with anomalies of opposite sign being attached to the western coast of the North America (Figs. 8a,d). This SST pattern closely resembles that of the PDO (Mantua et al. 1997). The overlying MD SLP patterns in the North Pacific are characterized by the Aleutian low variations with a single SLP anomaly center around the Aleutian Islands (Figs. 8b,e), which is another well-recognized feature for the PDO (e.g., Mantua et al. 1997; Mantua and Hare 2002). The correspondence between the PDO and the Aleutian low not only holds well on interannual time scales but also is robust on the MD time scale as discussed by Minobe (2000) and Zhu and Yang (2003). For example, the 1976/77 PDO regime shift from the negative to the positive phase was accompanied by the deepening of the Aleutian low (e.g., Zhang et al. 1997; Deser et al. 2004).

The corresponding MD wind patterns are generally in geostrophic balance with the MD SLP patterns

(Fig. 8). Over the North Pacific, the weakening of the Aleutian low corresponds to an anomalous anticyclone. The SLP low anomaly center over the western TP sets up zonal SLP gradient along the equator and thus leads to easterly wind anomalies. The subtropical trade winds blowing from northeast (southeast) in the Northern (Southern) Hemisphere also intensify as a result of the relatively higher SLP over the subtropics. The overall intensifications of the TP trade winds on the MD time scale induce positive–negative west–east sea level seesaw in the TP (Figs. 5d–f), similar to the observed wind and sea level trends during the altimeter period (e.g., Merrifield 2011; Merrifield and Maltrud 2011; McGregor et al. 2012; Qiu and Chen 2012). These anomalous wind patterns associated with the MD sea level mode resemble those during the negative phase of the PDO (e.g., Merrifield et al. 2012; Moon et al. 2013; Moon and Song 2016). The MD sea level PC1 with the turning point in the late 1980s is also consistent with the MD component of the PDO (not shown) or IPO index (Fig. 3c). Therefore, we can conclude that the MD sea level mode can be linked to the MD component of the ENSO-like variability in the Pacific, which could be regarded as the basin-scale expression of the North Pacific PDO.

c. Implications

Identifying the distinct temporal and spatial features as well as associated climate processes for QD and MD sea level modes have important implications in understanding both the basin-scale and regional low-frequency sea level variations in the Pacific. In previous studies the low-frequency sea level variations around the Pacific basin were usually linked to the NPGO or PDO. For example, Merrifield (2011) found that the tide gauge sea level records in the western TP and along the western coast of North America, after applying a 5-yr running average (thus including both QD and MD signals), are more correlated with the NPGO than with the PDO. In contrast, several studies (e.g., Bromirski et al. 2011; Merrifield et al. 2012; Moon et al. 2013) have suggested the MD sea level trend reversals in these two regions are linked to the PDO. Such discrepancy can be reconciled by our finding that the NPGO and PDO have different preferred time scales (i.e., QD and MD, respectively). A recent study by Moon and Song (2016) found that the low-frequency sea level variations in the East China Sea during the past half century comprise the PDO-related MD trend reversal and the NPGO-related QD signals. These regional evidences clearly indicate the frequency-dependent associations of the Pacific regional sea level with the NPGO and PDO, which to some extent represent the Pacific QD and MD climate variability modes, respectively.

5. ENSO-like low-frequency variability: Frequency-dependent features

a. ENSO-like low-frequency variability: QD and MD modes

In the previous section, we found that the Pacific basin QD and MD sea level modes are closely related to the ENSO-like low-frequency variability but also exhibit different patterns for various climate variables on these two time scales. This section aims to provide independent evidence that the QD and MD components of the ENSO-like low-frequency variability in the Pacific are indeed distinct from each other in both spatial patterns and physical mechanisms. The SVD analyses of SST and SLP were conducted to identify the dominant atmosphere–ocean coupled mode on different time scales based on the relatively longer ERSST and NOAA CIRES 20CR datasets. We have repeated our analysis using the Met Office Hadley Centre Sea Ice and Sea Surface Temperature dataset (HadISST; Rayner et al. 2003) and the ECMWF twentieth-century reanalysis (ERA-20C; Stickler et al. 2014) and found very similar features (not shown).
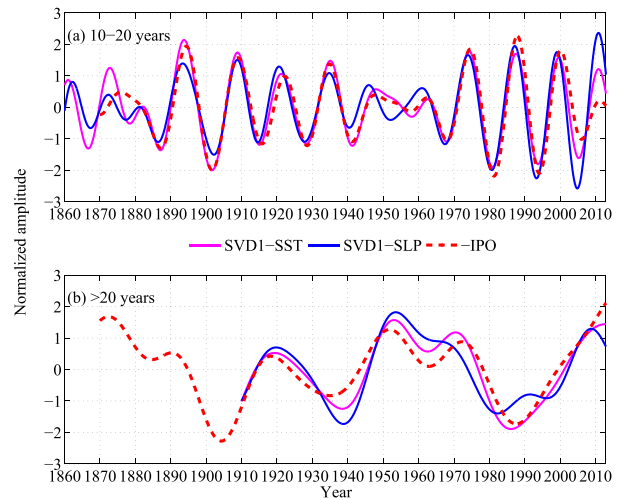

FIG. 9. The SVD1 time series of SST and SLP in the Pacific on time scales (a) between 10 and 20 yr and (b) >20 yr. The reversed IPO index time series on corresponding time scales are also shown (red dashed lines).

We repeated the SVD analysis with the 10–20-yr bandpass-filtered SST and SLP in the Pacific over 1860–2012 to identify the QD mode. Although using the 7–30-yr bandpass-filtered data as in the previous two sections yields similar SVD1 patterns, here a narrower period band (10–20 years) was chosen to rule out the influence of signals on other time scales (e.g., bidecadal). Both the SVD1 SST time series and the 10–20-yr bandpass-filtered IPO index (Henley et al. 2015) have a single spectral peak of approximately 13 yr on the QD time scale (not shown), and their temporal correlation is as high as −0.93 (Fig. 9a). This SVD1 thus represents the QD mode of the ENSO-like variability in the Pacific. The 10–20-yr SVD1 SST and SLP patterns (Figs. 10a,b) are very close to those associated with the Pacific QD sea level mode (Fig. 6). The distinctive features for the ENSO-like QD variability include the SST anomalies in the TP that are centered toward the central basin, an NPO-like SLP dipole and the Victoria mode–like SST pattern in the North Pacific (Figs. 10a,b). This QD mode of ENSO-like variability is analogous to the central TP SST variability on interannual time scales [i.e., the central Pacific ENSO (Yu and Kao 2007; Kao and Yu 2009) or El Niño Modoki (Ashok et al. 2007), which has also been related to the NPO-like SLP pattern over the North Pacific (Yu and Kim 2011a; Yu et al. 2012)]. The subtropical wind forcing in association with the southern pole of the NPO-like SLP dipole (see Figs. 6e,f) may be capable of inducing SST anomalies in the central TP, probably via the subtropical air–sea coupling (viz., the meridional mode; Yu et al. 2010; Yu and Kim 2011a) or through the recharge–discharge of the tropical heat content (Anderson et al. 2013). These
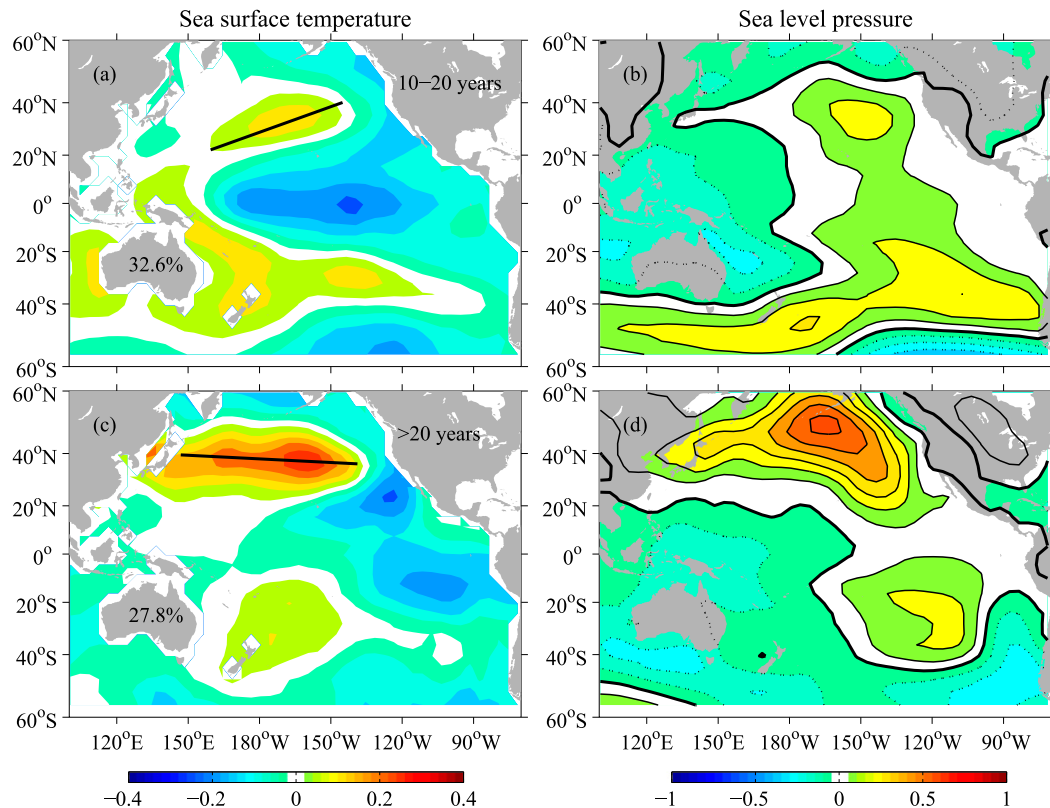
FIG. 10. The ENSO-like QD variability patterns, derived as the SVD1 patterns of 10–20-yr bandpass-filtered (a) SST (°C) and (b) SLP (hPa) in the Pacific over 1860–2012. (c),(d) As in (a),(b), but for the ENSO-like MD variability patterns, derived as the SVD1 patterns of 20-yr low-pass-filtered SST and SLP in the Pacific over 1910–2012. The data are from the ERSST and the NOAA CIRES 20CR. In (a),(c), the black lines mark the orientation of SST anomalies in the central–western North Pacific. The percentages in (a),(c) represent the percent of variance explained by the SVD1.

two mechanisms can also work on low-frequency time scales linking the extratropical North Pacific SLP forcing to the TP SST variations (Jin et al. 2001; Wu et al. 2007). Luo and Yamagata (2001) and Luo et al. (2003) argued that the TP SST QD variations are more related with the air–sea interaction and ocean dynamics in the South Pacific. Besides the extratropical forcing of the tropical climate, the TP SST anomalies can excite atmospheric teleconnections that feed back to influence the extratropical region. For example, Di Lorenzo et al. (2010) and Furtado et al. (2012) suggested that the atmospheric teleconnections excited by the central TP SST variations could induce the extratropical North Pacific atmospheric circulation anomalies (i.e., the NPO), which are in turn integrated by the ocean to generate QD variations of the NPGO. Yu et al. (2015b) found that the central TP SST variations can also have significant influences on the Southern Hemisphere climate by modulating both the southern annular mode (SAM) and the Pacific–South American (PSA) pattern. These physical processes could act

together to sustain this QD mode of ENSO-like variability across the whole Pacific (Figs. 10a,b).

Note that the low-frequency modulation of ENSO properties (e.g., the intensity and spatial distribution) can also induce low-frequency changes in the TP mean state because of the residual effects. However, we would like to clarify that such ENSO-induced low-frequency variability is fundamentally different from the ENSO-like low-frequency variability discussed in this study. For example, Sun and Yu (2009) found that the EOF1 of 10–20-yr bandpass-filtered SST anomalies in the TP represents the ENSO-like QD variability similar to that shown here (Fig. 10a), while the second EOF is related to a 10–15-yr modulation of ENSO intensity (thus should be termed as ENSO-induced QD variability) and exhibits remarkably different pattern from the EOF1. The distinct features between the ENSO-like and ENSO-induced low-frequency variability were also found in global coupled climate models (e.g., Yu and Kim 2011b; Choi et al. 2013).

The SVD analysis was also performed with the 20-yr low-pass-filtered SST and SLP data in the Pacific over
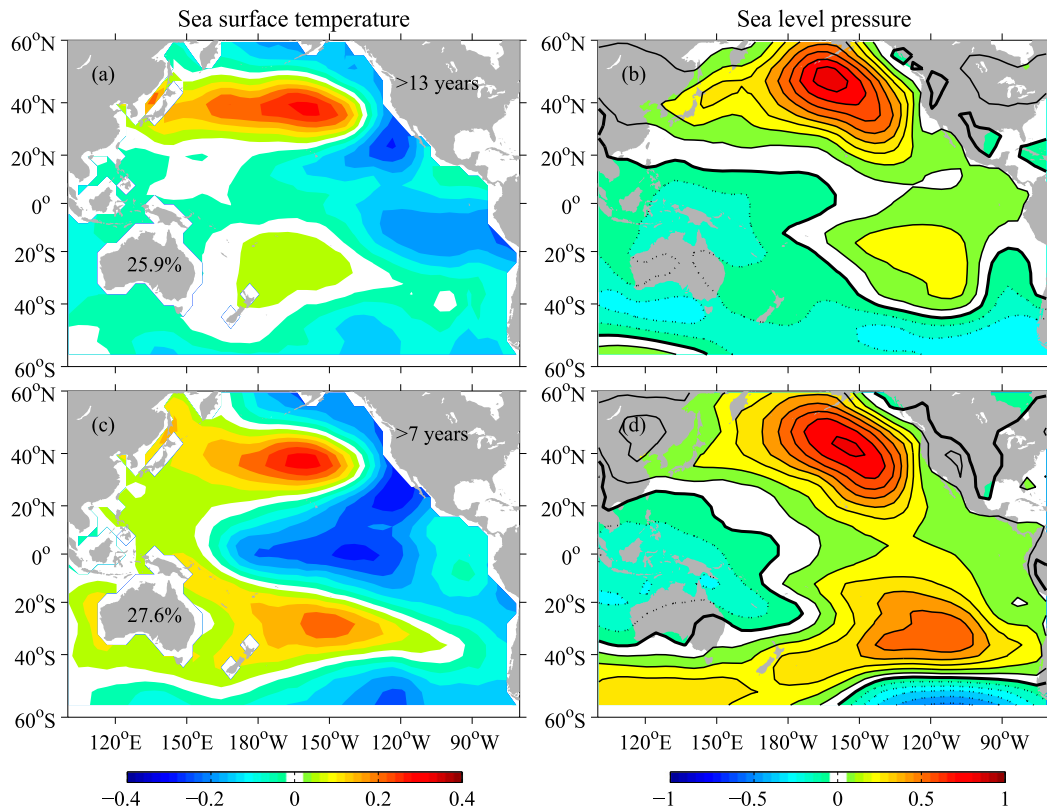
FIG. 11. As in Fig. 10, but over 1910–2012 on time scales (a),(b) >13 and (c),(d) >7 yr.

1910–2012 to identify the coupled MD mode. Using the cutoff period of 30 yr gives very similar results (not shown). The data before 1910 were not included here because the MD SVD1 time series based on the data over 1860–2012 has an abrupt change around 1910, probably because the data over the earlier period are less reliable or the long-term warming signal cannot be fully removed by a linear detrending. The correlation between the SVD1 SST time series and the 20-yr low-pass-filtered IPO index (Henley et al. 2015) is as high as −0.94 (Fig. 9b). This SVD1 thus represents the MD component of the ENSO-like variability in the Pacific. The MD SVD1 patterns have the same features as those associated with the MD sea level mode (Fig. 8), for example, the PDO-like SST pattern and the accompanying Aleutian low variations in the North Pacific and the TP SST anomalies toward the eastern basin or more specifically in the eastern subtropics (Figs. 10c,d). These MD patterns are also consistent with the observed difference patterns between the positive and negative MD climate regimes (e.g., Deser et al. 2004). This MD mode of ENSO-like variability is somewhat analogous to the conventional type of ENSO that has the maximum SST anomaly in the eastern TP, which is also related to the PDO and Aleutian low variations in the North Pacific on interannual time

scales (e.g., Yu and Kim 2011a). The origins of this ENSO-like MD variability are still unclear, while previous studies have offered some possible mechanisms that could determine the MD time scale in the Pacific, such as the subpolar ocean Rossby wave propagations (e.g., Liu 2012) or the remote forcing from the Atlantic (e.g., Zhang and Delworth 2007; Yu et al. 2015a; Lyu et al. 2017; Lyu and Yu 2017).

b. Comparison with previous studies: Interdecadal and low-frequency time scales

How do our findings of QD and MD modes relate to previous studies on the ENSO-like low-frequency variability? The 13-yr low-pass filter has usually been used to derive the smoothed IPO index and highlight the ENSO-like low-frequency variability on the interdecadal time scale (i.e., the IPO; Power et al. 1999; Folland et al. 1999, 2002; Henley et al. 2015). Such a cutoff frequency was originally chosen by Folland et al. (1999) to exclude the prominent QD signal in the Atlantic before the global SST EOF analysis. We found that the interdecadal SVD1 SST and SLP patterns based on the 13-yr low-pass-filtered data are nearly identical to those on the MD time scale with periods longer than 20 or 30 yr, except for larger amplitudes (Figs. 11a,b vs

Figs. 10c,d). The SVD1 SST time series and the IPO index are highly correlated (−0.91) on the interdecadal time scale with periods longer than 13 yr (not shown). It could be concluded that the widely used 13-yr low-pass-filtered IPO index implicitly rules out much of the ENSO-like variability on the QD time scale. This finding is consistent with Power et al. (1999), who defined the term interdecadal as the time scale with periods longer than both interannual and QD time scales.

It is also common to remove only interannual signals and examine the ENSO-like variability on lower frequencies (Zhang et al. 1997; Deser et al. 2012; Han et al. 2014; Chen and Wallace 2015; Lyu et al. 2016). The SVD1 SST time series based on the 7-yr low-pass-filtered data is highly correlated (−0.95) with the IPO index (not shown). Compared with the SVD1 on time scales longer than 13 or 20 yr (Figs. 11a,b or 10c,d), the SVD1 on time scales longer than 7 yr has different ENSO-like patterns: the subtropical eastern Pacific SST anomalies extend farther westward to the central TP, the SST and SLP anomalies in the midlatitude South Pacific are more zonally elongated, the North Pacific SLP anomaly center is located farther south, and there are larger SLP anomalies over the central TP (Figs. 11c,d). These features reflect some signatures from the ENSO-like QD variability (Figs. 10a,b) and indicate that the QD and MD signals merge into one single statistical mode when all low frequencies are considered simultaneously. Therefore, the ENSO-like low-frequency variability with periods longer than interannual time scales includes at least two distinct modes on QD and MD time scales, respectively, which have not been clearly distinguished in previous studies.

6. Summary and discussion

Zhang and Church (2012) suggested that the altimeter observed regional sea level trend pattern (Fig. 1a) may be partly due to the aliasing of the low-frequency climate variability into the trend. In this study, we analyzed the sea level data from satellite altimeter observations, ocean model hindcast simulations, ocean reanalysis, and steric sea level calculated based on in situ ocean observations to examine the low-frequency (>7 yr) sea level variations in the Pacific (section 3). Our results indicate that the dominant mode of low-frequency sea level variations in the Pacific basin exhibits both QD cycles and an MD trend reversal around the early 1990s (Fig. 3a). Further separating the QD and MD sea level signals we found that the sea level anomaly patterns on these two time scales show similar large-scale spatial distributions (i.e., the out-of-phase sea level variations roughly between the western and eastern sides of the

Pacific basin) but with different tropical structures. Sea level anomalies of opposite sign exist between the western and central TP with small anomalies in the far-eastern TP on the QD time scale, but there is a clear west–east sea level seesaw on the MD time scale (Figs. 5d–f vs Figs. 5a–c).

Distinguishing different spatial–temporal features for the QD and MD sea level variations explains why the dominant low-frequency sea level modes derived over different lengths of data periods show distinct spatial patterns (Figs. 1b, 2a–c vs Figs. 2d–f). It is found that while the sea level data over the altimeter period after 1993 sample about two QD cycles and roughly allow a clear identification of the QD sea level pattern (Figs. 1b and 2a–c), the relatively longer (~60 yr) datasets resolve both QD and MD sea level variations (Figs. 2d–f) with the latter appearing as a trend in the altimeter record (Fig. 1a). Our results suggest that the observed sea level variations as well as the derived short-term trends should be interpreted in the context of sea level variability on multiple time scales, which are linked to different climate processes and thus show distinct spatial patterns.

Such analyses of the sea level conducted in this study could be extended to other climate variables, especially those with data records only available for a short period. This is the case with some modern observation systems, such as the Argo floats since the early 2000s (Argo 2000), the Gravity Recovery and Climate Experiment (GRACE) since about 2002, and the satellite salinity measurements since about 2011. Taking the ocean salinity as an example, the Argo and buoy data show that the upper-ocean salinity in the TP experienced a QD shift during the 2000s (Hasegawa et al. 2013). In contrast, an MD trend reversal around the early to mid-1990s would become more evident when examining the tropical Indo-Pacific sea surface salinity using longer salinity records since the 1970s (Delcroix et al. 2007; Du et al. 2015; Zeng et al. 2016).

By examining the SST, SLP, and wind patterns in association with the low-frequency sea level variations (section 4), we found that both the QD and MD sea level modes in the Pacific basin can be viewed as expressions of the ENSO-like low-frequency climate variability (Zhang et al. 1997; Chen and Wallace 2015) in the sea level field. However, the associated climate patterns including SST, SLP, and wind differ significantly on these two time scales. The different TP sea level anomaly patterns on QD and MD time scales are in accordance with the contrasts between the corresponding surface wind forcing patterns. Additional analyses based on relatively longer SST and SLP data further confirm that the ENSO-like low-frequency variability in the Pacific is comprised of different subbasin expressions in both oceanic and atmospheric fields on QD and MD time scales,

respectively ([section 5](#)). The ENSO-like low-frequency variability on the QD time scale corresponding to the QD sea level mode in the Pacific is characterized by the central TP SST variations and the NPO-like ([Rogers 1981](#)) atmospheric forcing over the North Pacific, which has clear oceanic expressions resembling the NPGO ([Di Lorenzo et al. 2008](#)) and the SST Victoria mode ([Bond et al. 2003](#)) ([Figs. 10a,b](#)). In contrast, the ENSO-like low-frequency variability on the MD time scale, which corresponds to the MD sea level mode in the Pacific, exhibits the well-recognized PDO-like ([Mantua et al. 1997](#)) SST pattern and the accompanying Aleutian low variations in the North Pacific along with tropical Pacific SST anomalies mainly in the eastern basin ([Figs. 10c,d](#)).

Based on the results presented in this study, we conclude that the ENSO-like low-frequency variability in the Pacific on QD and MD time scales are distinct from each other in terms of the spatial patterns and also the climate processes involved. Our results refine the classical descriptions of the ENSO-like low-frequency variability, which identified only the interdecadal or equivalently MD patterns (e.g., [Folland et al. 1999](#), [2002](#); also shown in [Figs. 11a,b](#)) or patterns with mixed features from both QD and MD modes ([Zhang et al. 1997](#); [Chen and Wallace 2015](#), [2016](#); also shown in [Figs. 11c,d](#)). Several aspects of the ENSO-like low-frequency variability, including but not limited to the mechanisms, climate impacts, and interbasin connections, should be further reexamined under a frequency-dependent framework.

Distinguishing the low-frequency variability on different time scales could help to better understand the observed climate variations and to evaluate the potential predictability of the near-future climate. For example, [Wang et al. (2009](#), [2010](#), [2011](#), [2014)](#) showed that the climate signals in several regions of the United States, such as the rainfall over the Intermountain Region and the Missouri River basin water storage, have a significant QD time scale of 10–15 yr, which is distinct from the MD time scale of the PDO and could be linked to the ENSO-like QD SST variations. [Anderson et al. (2016b)](#) also found that the dominant time scales at which the precipitation variations are potentially predictable vary in different regions (e.g., the QD time scale over the northwestern United States and the MD time scale over the southwestern United States).

The PDO ([Mantua et al. 1997](#)) and NPGO ([Di Lorenzo et al. 2008](#)) have usually been viewed as two leading climate modes of the Pacific low-frequency variability. It needs to be recognized that both of them are locally defined EOF modes in the North Pacific or northeastern Pacific Ocean, while the ENSO-like low-frequency variability has been identified over the whole Pacific basin ([Zhang et al. 1997](#); [Chen and Wallace 2015](#)). Our results show that the NPGO and PDO, with preferred low-frequency time scales (i.e., QD and MD), could be regarded as regional expressions of the Pacific-basin ENSO-like low-frequency variability on respective time scales. Moreover, an EOF-based climate mode has its own shortcoming. The EOF decomposition assumes that for each EOF mode, one stationary spatial pattern fluctuates on various time scales that are included in the corresponding PC time series. However, a recent review by [Newman et al. (2016)](#) suggested that the PDO is not a single phenomenon but represents a combination of different dynamical processes that operate on different time scales and have distinct spatial structures.

While this study has clarified the main characteristics for the Pacific basin modes of low-frequency sea level variations and the associated wind forcing and climate processes, details about the concurrent changes in the ocean currents and subsurface ocean properties as well as the feedback of oceanic processes to the atmosphere require further investigations. It is also of great interest to check if the global coupled climate models can simulate the time-scale-dependent features of the ENSO-like low-frequency variability in the Pacific and the associated ocean and atmosphere coupled processes ([Lyu et al. 2016](#)), given that the realistic representation of the low-frequency variability is an important step to validate climate models and build up reliability of them to predict near-future climate.

REFERENCES

Anderson, B. T., R. C. Perez, and A. Karspeck, 2013: Triggering of El Niño onset through trade wind–induced charging of the equatorial Pacific. *Geophys. Res. Lett.*, **40**, 1212–1216, doi:10.1002/grl.50200.

——, D. J. S. Gianotti, J. C. Furtado, and E. Di Lorenzo, 2016a: A decadal precession of atmospheric pressures over the North Pacific. *Geophys. Res. Lett.*, **43**, 3921–3927, doi:10.1002/2016GL068206.

——, ——, G. Salvucci, and J. C. Furtado, 2016b: Dominant time scales of potentially predictable precipitation variations across

the continental United States. *J. Climate*, **29**, 8881–8897, doi:10.1175/JCLI-D-15-0635.1.

Argo, 2000: Argo float data and metadata from Global Data Assembly Centre (Argo GDAC). Sea Scientific Open Data Edition, doi:10.17882/42182.

Ashok, K., S. K. Behera, S. A. Rao, H. Weng, and T. Yamagata, 2007: El Niño Modoki and its possible teleconnection. *J. Geophys. Res.*, **112**, C11007, doi:10.1029/2006JC003798.

Balmaseda, M. A., K. Mogensen, and A. T. Weaver, 2013: Evaluation of the ECMWF ocean reanalysis system ORAS4. *Quart. J. Roy. Meteor. Soc.*, **139**, 1132–1161, doi:10.1002/qj.2063.

Behera, S. K., and T. Yamagata, 2010: Imprint of the El Niño Modoki on decadal sea level changes. *Geophys. Res. Lett.*, **37**, L23702, doi:10.1029/2010GL045936.

Bond, N. A., J. E. Overland, M. Spillane, and P. Stabeno, 2003: Recent shifts in the state of the North Pacific. *Geophys. Res. Lett.*, **30**, 2183, doi:10.1029/2003GL018597.

Brassington, G. B., 1997: The modal evolution of the Southern Oscillation. *J. Climate*, **10**, 1021–1034, doi:10.1175/1520-0442(1997)010<1021:TMEOTS>2.0.CO;2.

Bromirski, P. D., A. J. Miller, R. E. Flick, and G. Auad, 2011: Dynamical suppression of sea level rise along the Pacific coast of North America: Indications for imminent acceleration. *J. Geophys. Res.*, **116**, C07005, doi:10.1029/2010JC006759.

Capotondi, A., and M. A. Alexander, 2001: Rossby waves in the tropical North Pacific and their role in decadal thermocline variability. *J. Phys. Oceanogr.*, **31**, 3496–3515, doi:10.1175/1520-0485(2002)031<3496:RWITTN>2.0.CO;2.

——, ——, and C. Deser, 2003: Why are there Rossby wave maxima at 10°S and 13°N in the Pacific? *J. Phys. Oceanogr.*, **33**, 1549–1563, doi:10.1175/2407.1.

Carson, M., A. Köhl, and D. Stammer, 2015: The impact of regional multidecadal and century-scale internal climate variability on sea level trends in CMIP5 models. *J. Climate*, **28**, 853–861, doi:10.1175/JCLI-D-14-00359.1.

Chambers, M. A. M., M. A. Merrifield, and R. S. Nerem, 2012: Is there a 60-year oscillation in global mean sea level? *Geophys. Res. Lett.*, **39**, L18607, doi:10.1029/2012GL052885.

Chen, X., and J. M. Wallace, 2015: ENSO-like variability: 1900–2013. *J. Climate*, **28**, 9623–9641, doi:10.1175/JCLI-D-15-0322.1.

——, and ——, 2016: Orthogonal PDO and ENSO indices. *J. Climate*, **29**, 3883–3892, doi:10.1175/JCLI-D-15-0684.1.

Choi, J., S.-I. An, S.-W. Yeh, and J.-Y. Yu, 2013: ENSO-like and ENSO-induced tropical Pacific decadal variability in CGCMs. *J. Climate*, **26**, 1485–1501, doi:10.1175/JCLI-D-12-00118.1.

Church, J. A., and N. J. White, 2011: Sea-level rise from the late 19th to the early 21st century. *Surv. Geophys.*, **32**, 585–602, doi:10.1007/s10712-011-9119-1.

——, D. Monselesan, J. M. Gregory, and B. Marzeion, 2013: Evaluating the ability of process based models to project sea-level change. *Environ. Res. Lett.*, **8**, 014051, doi:10.1088/1748-9326/8/1/014051.

Compo, G. P., and Coauthors, 2011: The Twentieth Century Reanalysis project. *Quart. J. Roy. Meteor. Soc.*, **137**, 1–28, doi:10.1002/qj.776.

——, and Coauthors, 2015: NOAA-CIRES 20th Century Reanalysis version 2c. NOAA/ESRL/PSD, accessed 1 February 2016. [Available online at https://www.esrl.noaa.gov/psd/data/gridded/data.20thC_ReanV2c.html.]

CSIRO Sea Level Group, 2015: Combined TOPEX/Poseidon, *Jason-1* and *Jason-2*/OSTM sea level fields. CSIRO, accessed 17 June 2015. [Available online at http://www.cmar.csiro.au/sealevel/sl_data_cmar.html.]

Dangendorf, S., M. Marcos, A. Müller, E. Zorita, R. Riva, K. Berk, and J. Jensen, 2015: Detecting anthropogenic footprint in sea level rise. *Nat. Commun.*, **6**, 7849, doi:10.1038/ncomms8849.

Delcroix, T., S. Cravatte, and M. J. McPhaden, 2007: Decadal variations and trends in tropical Pacific sea surface salinity since 1970. *J. Geophys. Res.*, **112**, C03012, doi:10.1029/2006JC003801.

Deser, C., A. S. Phillips, and J. W. Hurrell, 2004: Pacific interdecadal climate variability: Linkages between the tropics and the North Pacific during boreal winter since 1900. *J. Climate*, **17**, 3109–3124, doi:10.1175/1520-0442(2004)017<3109:PICVLB>2.0.CO;2.

——, and Coauthors, 2012: ENSO and Pacific decadal variability in the Community Climate System Model version 4. *J. Climate*, **25**, 2622–2651, doi:10.1175/JCLI-D-11-00301.1.

Di Lorenzo, E., and Coauthors, 2008: North Pacific Gyre Oscillation links ocean climate and ecosystem change. *Geophys. Res. Lett.*, **35**, L08607, doi:10.1029/2007GL032838.

——, K. M. Cobb, J. C. Furtado, N. Schneider, B. T. Anderson, A. Bracco, M. A. Alexander, and D. J. Vimont, 2010: Central Pacific El Niño and decadal climate change in the North Pacific. *Nat. Geosci.*, **3**, 762–765, doi:10.1038/ngeo984.

——, and Coauthors, 2013: Synthesis of Pacific Ocean climate and ecosystem dynamics. *Oceanography*, **26**, 68–81, doi:10.5670/oceanog.2013.76.

Ding, R., J. Li, Y.-h. Tseng, C. Sun, and Y. Guo, 2015: The Victoria mode in the North Pacific linking extratropical sea level pressure variations to ENSO. *J. Geophys. Res. Atmos.*, **120**, 27–45, doi:10.1002/2014JD022221.

Du, Y., Y. Zhang, M. Feng, T. Wang, N. Zhang, and S. Wijffels, 2015: Decadal trends of the upper ocean salinity in the tropical Indo-Pacific since mid-1990s. *Sci. Rep.*, **5**, 16050, doi:10.1038/srep16050.

Duchon, C. E., 1979: Lanczos filtering in one and two dimensions. *J. Appl. Meteor.*, **18**, 1016–1022, doi:10.1175/1520-0450(1979)018<1016:LFIOAT>2.0.CO;2.

ECMWF, 2012: ECMWF Ocean Reanalysis System 4 (ORAS4). Integrated Climate Data Center, Ocean Synthesis/Reanalysis Directory, accessed 4 March 2016. [Available online at ftp://ftp.icdc.zmaw.de/EASYInit/ORA-S4/.]

Feng, M., Y. Li, and G. Meyers, 2004: Multidecadal variations of Fremantle sea level: Footprint of climate variability in the tropical Pacific. *Geophys. Res. Lett.*, **31**, L16302, doi:10.1029/2004GL019947.

——, M. J. McPhaden, and T. Lee, 2010: Decadal variability of the Pacific subtropical cells and their influence on the southeast Indian Ocean. *Geophys. Res. Lett.*, **37**, L09606, doi:10.1029/2010GL042796.

——, C. Boning, A. Biastoch, E. Behrens, E. Weller, and Y. Masumoto, 2011: The reversal of the multi-decadal trends of the equatorial Pacific easterly winds, and the Indonesian Throughflow and Leeuwin Current transports. *Geophys. Res. Lett.*, **38**, L11604, doi:10.1029/2011GL047291.

Folland, C. K., D. E. Parker, A. Colman, and R. Washington, 1999: Large scale modes of ocean surface temperature since the late nineteenth century. *Beyond El Niño: Decadal and Interdecadal Climate Variability*, A. Navarra, Ed., Springer, 73–102, doi:10.1007/978-3-642-58369-8_4.

——, J. A. Renwick, M. J. Salinger, and A. B. Mullan, 2002: Relative influences of the interdecadal Pacific oscillation and ENSO on the South Pacific convergence zone. *Geophys. Res. Lett.*, **29**, 1643, doi:10.1029/2001GL014201.

Frankcombe, L. M., S. McGregor, and M. H. England, 2015: Robustness of the modes of Indo-Pacific sea level variability. *Climate Dyn.*, **45**, 1281–1298, doi:10.1007/s00382-014-2377-0.

FRCGC/JAMSTEC, 2005: Subsurface temperature and salinity analyses by Ishii et al. NCAR Computational and Information Systems Laboratory Research Data Archive, accessed 23 February 2016. [Available online at http://rda.ucar.edu/datasets/ds285.3/.]

Furtado, J., E. DiLorenzo, B. Anderson, and N. Schneider, 2012: Linkages between the North Pacific Oscillation and central tropical Pacific SSTs at low frequencies. *Climate Dyn.*, **39**, 2833–2846, doi:10.1007/s00382-011-1245-4.

Hamlington, B. D., M. W. Strassburg, R. R. Leben, W. Han, R. S. Nerem, and K.-Y. Kim, 2014: Uncovering an anthropogenic sea-level rise signal in the Pacific Ocean. *Nat. Climate Change*, **4**, 782–785, doi:10.1038/nclimate2307.

——, S. H. Cheon, P. R. Thompson, M. A. Merrifield, R. S. Nerem, R. R. Leben, and K.-Y. Kim, 2016: An ongoing shift in Pacific Ocean sea level. *J. Geophys. Res. Oceans*, **121**, 5084–5097, doi:10.1002/2016JC011815.

Han, W., and Coauthors, 2014: Intensification of decadal and multidecadal sea level variability in the western tropical Pacific during recent decades. *Climate Dyn.*, **43**, 1357–1379, doi:10.1007/s00382-013-1951-1.

——, G. A. Meehl, D. Stammer, A. Hu, B. Hamlington, J. Kenigson, H. Palanisamy, and P. Thompson, 2017: Spatial patterns of sea level variability associated with natural internal climate modes. *Surv. Geophys.*, **38**, 217–250, doi:10.1007/s10712-016-9386-y.

Hasegawa, T., and K. Hanawa, 2003: Decadal-scale variability of upper ocean heat content in the tropical Pacific. *Geophys. Res. Lett.*, **30**, 1272, doi:10.1029/2002GL016843.

——, K. Ando, I. Ueki, K. Mizuno, and S. Hosoda, 2013: Upper-ocean salinity variability in the tropical Pacific: Case study for quasi-decadal shift during the 2000s using TRITON buoys and Argo floats. *J. Climate*, **26**, 8126–8138, doi:10.1175/JCLI-D-12-00187.1.

Henley, B. J., J. Gergis, D. J. Karoly, S. B. Power, J. Kennedy, and C. K. Folland, 2015: A tripole index for the interdecadal Pacific oscillation. *Climate Dyn.*, **45**, 3077–3090, doi:10.1007/s00382-015-2525-1.

Holbrook, N. J., I. D. Goodwin, S. McGregor, E. Molina, and S. B. Power, 2011: ENSO to multi-decadal time scale changes in East Australian Current transports and Fort Denison sea level: Oceanic Rossby waves as the connecting mechanism. *Deep-Sea Res. II*, **58**, 547–558, doi:10.1016/j.dsr2.2010.06.007.

Hu, A., and C. Deser, 2013: Uncertainty in future regional sea level rise due to internal climate variability. *Geophys. Res. Lett.*, **40**, 2768–2772, doi:10.1002/grl.50531.

Ishii, M., and M. Kimoto, 2009: Reevaluation of historical ocean heat content variations with time-varying XBT and MBT depth bias corrections. *J. Oceanogr.*, **65**, 287–299, doi:10.1007/s10872-009-0027-7.

JAMSTEC, 2015: Ocean General Circulation Model for the Earth Simulator (OFES). JAMSTEC, accessed 12 February 2015. [Available online at http://www.jamstec.go.jp/esc/fes/dods/OFES/OFES_NCEP_RUN/.]

Jin, F.-F., M. Kimoto, and X. Wang, 2001: A model of decadal ocean-atmosphere interaction in the North Pacific basin. *Geophys. Res. Lett.*, **28**, 1531–1534, doi:10.1029/2000GL008478.

JMA, 2013: JRA-55: Japanese 55-year Reanalysis, monthly means and variances. NCAR Computational and Information Systems Laboratory Research Data Archive, accessed 23 June 2016. [Available online at https://doi.org/10.5065/D60G3H5B.]

Kalnay, E., and Coauthors, 1996: The NCEP/NCAR 40-Year Reanalysis Project. *Bull. Amer. Meteor. Soc.*, **77**, 437–471, doi:10.1175/1520-0477(1996)077<0437:TNYRP>2.0.CO;2.

Kao, H.-Y., and J.-Y. Yu, 2009: Contrasting eastern-Pacific and central-Pacific types of ENSO. *J. Climate*, **22**, 615–632, doi:10.1175/2008JCLI2309.1.

Knutson, T., and S. Manabe, 1998: Model assessment of decadal variability and trends in the tropical Pacific Ocean. *J. Climate*, **11**, 2273–2296, doi:10.1175/1520-0442(1998)011<2273:MAODVA>2.0.CO;2.

Kobayashi, S., and Coauthors, 2015: The JRA-55 reanalysis: General specifications and basic characteristics. *J. Meteor. Soc. Japan*, **93**, 5–48, doi:10.2151/jmsj.2015-001.

Köhl, A., 2014: Detecting processes contributing to interannual halosteric and thermosteric sea level variability. *J. Climate*, **27**, 2417–2426, doi:10.1175/JCLI-D-13-00412.1.

Lee, T., and M. J. McPhaden, 2008: Decadal phase change in large-scale sea level and winds in the Indo-Pacific region at the end of the 20th century. *Geophys. Res. Lett.*, **35**, L01605, doi:10.1029/2007GL032419.

Li, Y., and W. Han, 2015: Decadal sea level variations in the Indian Ocean investigated with HYCOM: Roles of climate modes, ocean internal variability, and stochastic wind forcing. *J. Climate*, **28**, 9143–9165, doi:10.1175/JCLI-D-15-0252.1.

Liu, Z., 2012: Dynamics of interdecadal climate variability: A historical perspective. *J. Climate*, **25**, 1963–1995, doi:10.1175/2011JCLI3980.1.

Lohmann, K., and M. Latif, 2005: Tropical Pacific decadal variability and the subtropical–tropical cells. *J. Climate*, **18**, 5163–5178, doi:10.1175/JCLI3559.1.

Luo, J.-J., and T. Yamagata, 2001: Long-term El Niño-Southern Oscillation (ENSO)-like variation with special emphasis on the South Pacific. *J. Geophys. Res.*, **106**, 22 211–22 227, doi:10.1029/2000JC000471.

——, S. Masson, S. Behera, P. Delecluse, S. Gualdi, A. Navarra, and T. Yamagata, 2003: South Pacific origin of the decadal ENSO-like variation as simulated by a coupled GCM. *Geophys. Res. Lett.*, **30**, 2250, doi:10.1029/2003GL018649.

Lyu, K., and J.-Y. Yu, 2017: Climate impacts of the Atlantic multidecadal oscillation simulated in the CMIP5 models: A re-evaluation based on a revised index. *Geophys. Res. Lett.*, **44**, doi:10.1002/2017GL072681, in press.

——, X. Zhang, J. A. Church, A. B. A. Slangen, and J. Hu, 2014: Time of emergence for regional sea-level change. *Nat. Climate Change*, **4**, 1006–1010, doi:10.1038/nclimate2397.

——, ——, ——, and J. Hu, 2015: Quantifying internally generated and externally forced climate signals at regional scales in CMIP5 models. *Geophys. Res. Lett.*, **42**, 9394–9403, doi:10.1002/2015GL065508.

——, ——, ——, and ——, 2016: Evaluation of the interdecadal variability of sea surface temperature and sea level in the Pacific in CMIP3 and CMIP5 models. *Int. J. Climatol.*, **36**, 3723–3740, doi:10.1002/joc.4587.

——, J.-Y. Yu, and H. Paek, 2017: The influences of the Atlantic multidecadal oscillation on the mean strength of the North Pacific subtropical high during boreal winter. *J. Climate*, **30**, 411–426, doi:10.1175/JCLI-D-16-0525.1.

Mantua, N. J., and S. R. Hare, 2002: The Pacific decadal oscillation. *J. Oceanogr.*, **58**, 35–44, doi:10.1023/A:1015820616384.

——, ——, Y. Zhang, J. M. Wallace, and R. C. Francis, 1997: A Pacific interdecadal climate oscillation with impacts on salmon production. *Bull. Amer. Meteor. Soc.*, **78**, 1069–1079, doi:10.1175/1520-0477(1997)078<1069:APICOW>2.0.CO;2.

McGregor, S., A. S. Gupta, and M. H. England, 2012: Constraining wind stress products with sea surface height observations and implications for Pacific Ocean sea level

trend attribution. *J. Climate*, **25**, 8164–8176, doi:10.1175/JCLI-D-12-00105.1.

Merrifield, M. A., 2011: A shift in western tropical Pacific sea level trends during the 1990s. *J. Climate*, **24**, 4126–4138, doi:10.1175/2011JCLI3932.1.

——, and M. E. Maltrud, 2011: Regional sea level trends due to a Pacific trade wind intensification. *Geophys. Res. Lett.*, **38**, L21605, doi:10.1029/2011GL049576.

——, P. R. Thompson, and M. Lander, 2012: Multidecadal sea level anomalies and trends in the western tropical Pacific. *Geophys. Res. Lett.*, **39**, L13602, doi:10.1029/2012GL052032.

Meyssignac, B., D. Salas y Melia, M. Becker, W. Llovel, and A. Cazenave, 2012: Tropical Pacific spatial trend patterns in observed sea level: Internal variability and/or anthropogenic signature? *Climate Past*, **8**, 787–802, doi:10.5194/cp-8-787-2012.

Minobe, S., 1997: A 50–70 year climatic oscillation over the North Pacific and North America. *Geophys. Res. Lett.*, **24**, 683–686, doi:10.1029/97GL00504.

——, 1999: Resonance in bidecadal and pentadecadal climate oscillations over the North Pacific: Role in climatic regime shifts. *Geophys. Res. Lett.*, **26**, 855–858, doi:10.1029/1999GL900119.

——, 2000: Spatio-temporal structure of the pentadecadal variability over the North Pacific. *Prog. Oceanogr.*, **47**, 381–408, doi:10.1016/S0079-6611(00)00042-2.

Moon, J.-H., and Y. T. Song, 2016: Decadal sea level variability in the East China Sea linked to the North Pacific Gyre Oscillation. *Cont. Shelf Res.*, doi:10.1016/j.csr.2016.05.003, in press.

——, ——, P. D. Bromirski, and A. J. Miller, 2013: Multi-decadal regional sea level shifts in the Pacific over 1958–2008. *J. Geophys. Res. Oceans*, **118**, 7024–7035, doi:10.1002/2013JC009297.

——, ——, and H. Lee, 2015: PDO and ENSO modulations intensified decadal sea level variability in the tropical Pacific. *J. Geophys. Res. Oceans*, **120**, 8229–8237, doi:10.1002/2015JC011139.

Newman, M., and Coauthors, 2016: The Pacific decadal oscillation, revisited. *J. Climate*, **29**, 4399–4427, doi:10.1175/JCLI-D-15-0508.1.

Nidheesh, A., M. Lengaigne, J. Vialard, A. Unnikrishnan, and H. Dayan, 2013: Decadal and long-term sea level variability in the tropical Indo-Pacific Ocean. *Climate Dyn.*, **41**, 381–402, doi:10.1007/s00382-012-1463-4.

NOAA/NCEI, 2015: NOAA Extended Reconstructed Sea Surface Temperature version 4. NOAA/ESRL/PSD, accessed 10 August 2016. [Available online at https://www.esrl.noaa.gov/psd/data/gridded/data.noaa.ersst.v4.html.]

NOAA/NCEP, 1994: NCEP/NCAR reanalysis monthly means and other derived variables. NOAA/ESRL/PSD, accessed 11 February 2016. [Available online at https://www.esrl.noaa.gov/psd/data/gridded/data.ncep.reanalysis.derived.html.]

Palanisamy, H., A. Cazenave, T. Delcroix, and B. Meyssignac, 2015a: Spatial trend patterns in the Pacific Ocean sea level during the altimetry era: The contribution of thermocline depth change and internal climate variability. *Ocean Dyn.*, **65**, 341–356, doi:10.1007/s10236-014-0805-7.

——, B. Meyssignac, A. Cazenave, and T. Delcroix, 2015b: Is anthropogenic sea level fingerprint already detectable in the Pacific Ocean? *Environ. Res. Lett.*, **10**, 084024, doi:10.1088/1748-9326/10/8/084024.

Power, S., T. Casey, C. Folland, A. Colman, and V. Mehta, 1999: Inter-decadal modulation of the impact of ENSO on Australia. *Climate Dyn.*, **15**, 319–324, doi:10.1007/s003820050284.

Qiu, B., 2003: Kuroshio Extension variability and forcing of the Pacific decadal oscillations: Responses and potential feedback. *J. Phys. Oceanogr.*, **33**, 2465–2482, doi:10.1175/2459.1.

——, and S. Chen, 2006: Decadal variability in the large-scale sea surface height field of the South Pacific Ocean: Observations and causes. *J. Phys. Oceanogr.*, **36**, 1751–1762, doi:10.1175/JPO2943.1.

——, and ——, 2012: Multidecadal sea level and gyre circulation variability in the northwestern tropical Pacific Ocean. *J. Phys. Oceanogr.*, **42**, 193–206, doi:10.1175/JPO-D-11-061.1.

——, N. Schneider, and S. Chen, 2007: Coupled decadal variability in the North Pacific: An observationally constrained idealized model. *J. Climate*, **20**, 3602–3620, doi:10.1175/JCLI4190.1.

——, S. Chen, L. Wu, and S. Kida, 2015: Wind- versus eddy-forced regional sea level trends and variability in the North Pacific Ocean. *J. Climate*, **28**, 1561–1577, doi:10.1175/JCLI-D-14-00479.1.

Rayner, N. A., D. E. Parker, E. B. Horton, C. K. Folland, L. V. Alexander, D. P. Rowell, E. C. Kent, and A. Kaplan, 2003: Global analyses of sea surface temperature, sea ice, and night marine air temperatures since the late nineteenth century. *J. Geophys. Res.*, **108**, 4407, doi:10.1029/2002JD002670.

Rogers, J. C., 1981: The North Pacific Oscillation. *J. Climatol.*, **1**, 39–57, doi:10.1002/joc.3370010106.

Sasaki, H., and Coauthors, 2004: A series of eddy-resolving ocean simulations in the World Ocean: OFES (OGCM for the Earth Simulator) project. *Proc. OCEANS'04/TECHNO-OCEAN'04*, Kobe, Japan, MTS and IEEE, 1535–1541.

——, M. Nonaka, Y. Masumoto, Y. Sasai, H. Uehara, and H. Sakuma, 2008: An eddy-resolving hindcast simulation of the quasiglobal ocean from 1950 to 2003 on the Earth Simulator. *High Resolution Numerical Modelling of the Atmosphere and Ocean*, W. Ohfuchi and K. Hamilton, Eds., Springer, 157–186.

Sasaki, Y., S. Minobe, N. Schneider, T. Kagimoto, M. Nonaka, and H. Sasaki, 2008: Decadal sea level variability in the South Pacific in a global eddy-resolving ocean model hindcast. *J. Phys. Oceanogr.*, **38**, 1731–1747, doi:10.1175/2007JPO3915.1.

Sérazin, G., B. Meyssignac, T. Penduff, L. Terray, B. Barnier, and J.- M. Molines, 2016: Quantifying uncertainties on regional sea level change induced by multidecadal intrinsic oceanic variability. *Geophys. Res. Lett.*, **43**, 8151–8159, doi:10.1002/2016GL069273.

Slangen, A. B. A., J. A. Church, C. Agosta, X. Fettweis, B. Marzeion, and K. Richter, 2016: Anthropogenic forcing dominates global mean sea-level rise since 1970. *Nat. Climate Change*, **6**, 701–705, doi:10.1038/nclimate2991.

Smith, T. M., R. W. Reynolds, T. C. Peterson, and J. Lawrimore, 2008: Improvements to NOAA's historical merged land–ocean surface temperature analysis (1880–2006). *J. Climate*, **21**, 2283–2296, doi:10.1175/2007JCLI2100.1.

Stammer, D., A. Cazenave, R. M. Ponte, and M. E. Tamisiea, 2013: Causes for contemporary regional sea level changes. *Annu. Rev. Mar. Sci.*, **5**, 21–46, doi:10.1146/annurev-marine-121211-172406.

Stickler, A., and Coauthors, 2014: ERA-CLIM: Historical surface and upper-air data for future reanalyses. *Bull. Amer. Meteor. Soc.*, **95**, 1419–1430, doi:10.1175/BAMS-D-13-00147.1.

Sullivan, A., J.-J. Luo, A. C. Hirst, D. Bi, W. Cai, and J. He, 2016: Robust contribution of decadal anomalies to the frequency of central-Pacific El Niño. *Sci. Rep.*, **6**, 38540, doi:10.1038/srep38540.

Sun, F., and J.-Y. Yu, 2009: A 10–15-yr modulation cycle of ENSO intensity. *J. Climate*, **22**, 1718–1735, doi:10.1175/2008JCLI2285.1.

Tourre, Y. M., B. Rajagopalan, Y. Kushnir, M. Barlow, and W. B. White, 2001: Patterns of coherent decadal and interdecadal climate signals in the Pacific basin during the 20th century. *Geophys. Res. Lett.*, **28**, 2069–2072, doi:10.1029/2000GL012780.

——, C. Cibot, L. Terray, W. B. White, and B. Dewitte, 2005: Quasi-decadal and inter-decadal climate fluctuations in the

Pacific Ocean from a CGCM. *Geophys. Res. Lett.*, **32**, L07710, doi:10.1029/2004GL022087.

Wallace, J. M., C. Smith, and C. S. Bretherton, 1992: Singular value decomposition of wintertime sea surface temperature and 500-mb height anomalies. *J. Climate*, **5**, 561–576, doi:10.1175/1520-0442(1992)005<0561:SVDOWS>2.0.CO;2.

Wang, S.-Y., R. R. Gillies, J. Jin, and L. E. Hipps, 2009: Recent rainfall cycle in the intermountain region as a quadrature amplitude modulation from the Pacific decadal oscillation. *Geophys. Res. Lett.*, **36**, L02705, doi:10.1029/2008GL036329.

——, ——, ——, and ——, 2010: Coherence between the Great Salt Lake level and the Pacific quasi-decadal oscillation. *J. Climate*, **23**, 2161–2177, doi:10.1175/2009JCLI2979.1.

——, ——, L. E. Hipps, and J. Jin, 2011: A transition-phase tele-connection of the Pacific quasi-decadal oscillation. *Climate Dyn.*, **36**, 681–693, doi:10.1007/s00382-009-0722-5.

——, K. Hakala, R. R. Gillies, and W. J. Capehart, 2014: The Pacific quasi-decadal oscillation (QDO): An important pre-cursor toward anticipating major flood events in the Missouri River basin? *Geophys. Res. Lett.*, **41**, 991–997, doi:10.1002/2013GL059042.

Weng, H., K. Ashok, S. K. Behera, S. A. Rao, and T. Yamagata, 2007: Impacts of recent El Niño Modoki on dry/wet conditions in the Pacific Rim during boreal summer. *Climate Dyn.*, **29**, 113–129, doi:10.1007/s00382-007-0234-0.

Widlansky, M. J., A. Timmermann, and W. Cai, 2015: Future ex-treme sea level seesaws in the tropical Pacific. *Sci. Adv.*, **1**, e1500560, doi:10.1126/sciadv.1500560.

Wu, L. X., Z. Y. Liu, C. Li, and Y. Sun, 2007: Extratropical control of recent tropical Pacific decadal climate variability: A relay teleconnection. *Climate Dyn.*, **28**, 99–112, doi:10.1007/s00382-006-0198-5.

Wu, Q., X. Zhang, J. A. Church, and J. Hu, 2017: Variability and change of sea level and its components in the Indo-Pacific region during the altimetry era. *J. Geophys. Res. Oceans*, **122**, 1862–1881, doi:10.1002/2016JC012345.

Yu, J.-Y., and H.-Y. Kao, 2007: Decadal changes of ENSO persistence barrier in SST and ocean heat content indices: 1958–2001. *J. Geophys. Res.*, **112**, D13106, doi:10.1029/2006JD007715.

——, and S. T. Kim, 2011a: Relationships between extratropical sea level pressure variations and the central Pacific and eastern Pacific types of ENSO. *J. Climate*, **24**, 708–720, doi:10.1175/2010JCLI3688.1.

——, and ——, 2011b: Reversed spatial asymmetries between El Niño and La Niña and their linkage to decadal ENSO modu-lation in CMIP3 models. *J. Climate*, **24**, 5423–5434, doi:10.1175/JCLI-D-11-00024.1.

——, H.-Y. Kao, and T. Lee, 2010: Subtropics-related interannual sea surface temperature variability in the central equatorial Pacific. *J. Climate*, **23**, 2869–2884, doi:10.1175/2010JCLI3171.1.

——, M.-M. Lu, and S. T. Kim, 2012: A change in the relationship between tropical central Pacific SST variability and the ex-tratropical atmosphere around 1990. *Environ. Res. Lett.*, **7**, 034025, doi:10.1088/1748-9326/7/3/034025.

——, P.-K. Kao, H. Paek, H.-H. Hsu, C.-W. Hung, M.-M. Lu, and S.-I. An, 2015a: Linking emergence of the central Pacific El Niño to the Atlantic multidecadal oscillation. *J. Climate*, **28**, 651–662, doi:10.1175/JCLI-D-14-00347.1.

——, H. Paek, E. S. Saltzman, and T. Lee, 2015b: The early 1990s change in ENSO–PSA–SAM relationships and its impact on Southern Hemisphere climate. *J. Climate*, **28**, 9393–9408, doi:10.1175/JCLI-D-15-0335.1.

Zeng, L., D. Wang, P. Xiu, Y. Shu, Q. Wang, and J. Chen, 2016: Decadal variation and trends in subsurface salinity from 1960 to 2012 in the northern South China Sea. *Geophys. Res. Lett.*, **43**, 12 181–12 189, doi:10.1002/2016GL071439.

Zhang, R., and T. L. Delworth, 2007: Impact of the Atlantic multi-decadal oscillation on North Pacific climate variability. *Geo-phys. Res. Lett.*, **34**, L23708, doi:10.1029/2007GL031601.

Zhang, X., and J. A. Church, 2012: Sea level trends, interannual and decadal variability in the Pacific Ocean. *Geophys. Res. Lett.*, **39**, L21701, doi:10.1029/2012GL053240.

——, B. Cornuelle, and D. Roemmich, 2012: Sensitivity of western boundary transport at the mean north equatorial current bi-furcation latitude to wind forcing. *J. Phys. Oceanogr.*, **42**, 2056–2072, doi:10.1175/JPO-D-11-0229.1.

——, J. A. Church, S. M. Plattern, and D. Monselesan, 2014: Pro-jection of subtropical gyre circulation and associated sea level changes in the Pacific based on CMIP3 climate models. *Cli-mate Dyn.*, **43**, 131–144, doi:10.1007/s00382-013-1902-x.

Zhang, Y., J. M. Wallace, and D. S. Battisti, 1997: ENSO-like in-terdecadal variability: 1900–93. *J. Climate*, **10**, 1004–1020, doi:10.1175/1520-0442(1997)010<1004:ELIV>2.0.CO;2.

Zhu, Y., and X. Yang, 2003: Joint propagating patterns of SST and SLP anomalies in the North Pacific on bidecadal and penta-decadal timescales. *Adv. Atmos. Sci.*, **20**, 694–710, doi:10.1007/BF02915396.